ACS Chemical Neuroscience

Article

PRENYLATED CURCUMIN ANALOGUES AS MULTIPOTENT TOOLS TO TACKLE ALZHEIMER'S DISEASE

Federica Bisceglia, Francesca Seghetti, Massimo Serra, Morena Zusso, Silvia Gervasoni, Laura Verga, Giulio Vistoli, Cristina Lanni, Michele Catanzaro, Ersilia De Lorenzi, and Federica Belluti

Just Accepted

ACS Publications

PRENYLATED CURCUMIN ANALOGUES AS MULTIPOTENT TOOLS TO TACKLE ALZHEIMER'S DISEASE

Federica Bisceglia [a], Francesca Seghetti [b], Massimo Serra[a], Morena Zusso [c], Silvia Gervasoni [d], Laura Verga [e], Giulio Vistoli [d], Cristina Lanni [a], Michele Catanzaro [a], Ersilia De Lorenzi *,[a], Federica Belluti [b]

[a] Department of Drug Sciences, University of Pavia, Viale Taramelli 12, 27100, Pavia, Italy.

[b] Department of Pharmacy and Biotechnology, *Alma Mater Studiorum*-University of Bologna, Via Belmeloro 6, 40126 Bologna, Italy.

[c] Department of Pharmaceutical and Pharmacological Sciences, University of Padua, Largo Meneghetti 2, 35131 Padua, Italy.

[d] Department of Pharmaceutical Sciences, University of Milan, Via Mangiagalli 25, 20133 Milan, Italy.

[e] Department of Molecular Medicine, Unit of Pathology, University of Pavia IRCCS Policlinico S. Matteo Foundation, Via Forlanini 14, 27100, Pavia, Italy.

1

ABSTRACT

Alzheimer's disease is likely to be caused by copathogenic factors including aggregation of Aβ peptides into oligomers and fibrils, neuroinflammation and oxidative stress. To date, no effective treatments are available and because of the multifactorial nature of the disease, it emerges the need to act on different and simultaneous fronts. Despite the multiple biological activities ascribed to curcumin as neuroprotector, its poor bioavailability and toxicity limit the success in clinical outcomes. To tackle Alzheimer's disease on these aspects, the curcumin template was suitably modified and a small set of analogues was attained. In particular, derivative **1** turned out to be less toxic than curcumin. As evidenced by capillary electrophoresis and transmission electron microscopy studies, **1** proved to inhibit the formation of large toxic Aβ oligomers, by shifting the equilibrium towards smaller non-toxic assemblies and to limit the formation of insoluble fibrils. These findings were supported by molecular docking and steered molecular dynamics simulations which confirmed the superior capacity of **1** to bind Aβ structures of different complexity. Remarkably, **1** also showed *in vitro* anti-inflammatory and anti-oxidant properties. In summary, the curcumin-based analogue **1** emerged as multipotent compound worth to be further investigated and exploited in the Alzheimer's disease multi-target context.

Keywords: Alzheimer's disease; amyloid beta oligomers and fibrils; capillary electrophoresis; curcumin analogues; neuroinflammation; oxidative stress.

INTRODUCTION

Alzheimer's disease (AD) is the most common form of dementia [1] and despite impressive efforts, so far the set up of a successful anti-AD drug discovery strategy resulted extremely difficult, mainly because of the multifactorial nature of the disease [1, 2]. In the last years, numerous AD-modifying therapeutics failed clinical trials and, to date, only five drugs mainly targeting cholinesterases have been approved by Food and Drug Administration. Compelling evidences consider extracellular amyloid-beta (Aβ) deposits in the brain as one of the main AD hallmarks [1, 3, 4]: they trigger microglia and astrocytes activation, which in turn results in chronic inflammation and cellular oxidative stress [3, 5, 6]. All these mechanisms, together with mithocondria and neurovascular dysfunctions, are mutually involved in a feed-forward loop, ultimately leading to progressive neurodegeneration [1, 6].

Aβ protein includes natively disordered peptides, ranging from 36 to 43 amino acids, that are produced from the sequential metabolism of amyloid precursor protein by β- and γ-secretases [4]; in particular, the predominant species found in plaques is the most toxic and amylodogenic $A\beta_{1-42}$ ($A\beta_{42}$). Monomeric $A\beta_{42}$ peptide is prone to self-assembly into oligomeric species, which aggregate to form protofibrils and then mature amyloid fibrils [2, 4]. Some well-defined Aβ peptide regions are involved in the aggregation process [7]. The glycosaminoglycan (GAGs) binding site (HHQK) assists, via a α-helix intermediate, the conformational transition of monomers from normal random coil to β-sheet structure which is characterized by an increased tendency to aggregate into dimers and oligomers [8]. The stabilization of the soluble Aβ monomers conformation, or the prevention of the α-to-β conformational transition, represent suitable strategies to avoid oligomers formation. The self recognition hydrophobic core ([16]KLVFFA[21]), located in the central region of Aβ peptide, constitutes a nucleation site that initiates the Aβ-Aβ interaction [9]. In particular, π-π stacking involving the two Phe residues may play a significant role in the self-assembly process. The emerging π-π-hypothesis suggests that drugs able to block these interactions may effectively control the amyloid diseases [10]. After this primary lag step, spherical oligomers transform into larger aggregates (nucleation phase) and an equilibrium between hydrophobic and hydrophilic interactions, involving Glu[22]-Gly[29] residues, is thought to affect this stage.

Notably, in the last 25 years attention has been shifted from amyloid fibrils to soluble prefibrillar Aβ oligomers which, unlike other amyloidoses, are found to be more toxic than mature fibrils [11]. $A\beta_{42}$ oligomers bind to hippocampal neurons and hamper synaptic plasticity, manifested as inhibition of the long-term potentiation, which is involved in learning and memory [4, 12]. To date, it is not clear which particular oligomeric state is mainly involved in eliciting neurotoxic effects and by which specific mechanism. Indeed, the transient and non-covalent nature makes it difficult their identification and characterization [2, 13, 14]. On the other hand, also insoluble fibril deposits are found to be neurotoxic since, being in equilibrium with oligomers, they may serve as a reservoir and catalyze oligomer formation through

3

secondary nucleation pathways. Consequently, both oligomers and fibrils represent important targets. In this scenario, a multitarget approach based on the simultaneous inhibition of some relevant AD targets offers promises to achieve a successful therapeutic outcome [15].

Curcumin (Figure 1), the primary bioactive compound found in the rhizome of *Curcuma longa*, has been reported to interfere with Aβ aggregation and to attenuate oxidative stress and neuroinflammation [16-18].

The 4-hydroxy,3-methoxy-phenyl (vanillin) rings of curcumin were shown to adopt a correct position to establish π-π interactions with Phe[19] and Phe[20] residues of Aβ [19-21], as a result of the appropriate length and flexibility of the heptatrienone central linker [22, 23]. In addition, the curcumin coplanar rearrangement allows the intercalation between the Aβ fibrils, thus hampering the β-sheets assembly and in turn the fibrillation pathways [20]. Nevertheless curcumin does not have success in clinical trials, due to its poor bioavailability and possible toxic effects, mainly ascribed to the 4-hydroxy,3-methoxy substitution pattern of the two aryl rings [22, 24]. Together with a large number of multipotent compounds such as quinones, cathecols, and isothiazolones, curcumin has been included among pan-assay interfering compounds (PAINS), since they can display apparent bioactivity and/or interfere with assay readouts [24, 25]. It is not definite whether compounds containing a PAINS-related sub-structure behave as reactive chemicals rather than selective drugs, indeed the reactivity of a compound or other effects might be also context-dependent [26]. However, a number of curcumin-based compounds, when properly decorated, have been shown to exert significant biological activities [21, 27], thus confirming the great potential of the curcumin scaffold for drug discovery. In this context, the key chemical features for an Aβ ligand have been identified to comprise two sterically bulky aromatic moieties, connected by a flexible linker of suitable length, to ensure their optimal spatial arrangement [23]. The resulting elongated and flat molecule demonstrated to hamper the characteristic π-π stacking interactions between the aromatic residues of Aβ monomers, oligomers, or filaments [19, 20].

In order to identify multipotent AD disease-modifying drug candidates [15, 28] with an improved biological profile as compared to the reference compound curcumin, a small series of newly synthesized analogues was here tested for anti-oligomeric and anti-fibrillogenic activity, while toxicity was evaluated on both neuroblastoma and microglia cells. Molecular docking and steered molecular dynamics (SMD) simulations were performed in order to assess the molecular recognition of the derivatives with either monomeric or aggregated Aβ$_{42}$ and to assess the stability of the corresponding complexes which are responsible for the inhibitory activity. The identification of probes able to modulate Aβ aggregation, inflammation and oxidative stress could allow to shed light into this cross-talk and represents a crucial issue in the AD drug discovery scenario. Therefore, the most promising compounds in terms of anti-oligomeric and anti-fibrillogenic activity were also evaluated for their anti-inflammatory and anti-oxidant properties.

RESULTS AND DISCUSSION

Design and synthesis of curcumin analogues. The aromatic 4-hydroxy,3-methoxy substitution patterns of curcumin (**cur**, Figure 1) were sequentially replaced with the *para*-3,3-dimethylallyloxy (4-prenyloxy), to obtain **1** as asymmetrical compound, bearing both vanillin and 4-prenyloxyphenyl functions, and **2** (Figure 1), as symmetrical counterpart in which both side rings were decorated with the 4-prenyloxy group. This moiety, found in a large number of natural products, proved to be often associated to neuroprotective effects, such as anti-inflammatory and anti-oxidant, among others [29, 30]. This flexible mono-unsaturated function could also impart to the molecule an increased capability to establish hydrophobic contacts with Aβ monomers. Furthermore, the importance of the hepta-1,4,6-trien-3-one central linker was studied by its proper simplification into a penta-1,4-dien-3-one, obtaining the corresponding compounds **3** and **4** (Figure 1). Since this structural modification has been successfully introduced in the design of curcumin derivatives with increased anti-proliferative and anti-inflammatory activities [31], we wondered if the same increased activity would have been observed in AD multi-target context. Indeed, the maintenance of the carbonyl α,β-unsaturated electrophile reactive centre, together with the length of the linker (6–19 Å) and its rigidity are some of the key chemical features required to effectively inhibit amyloid aggregation [23].
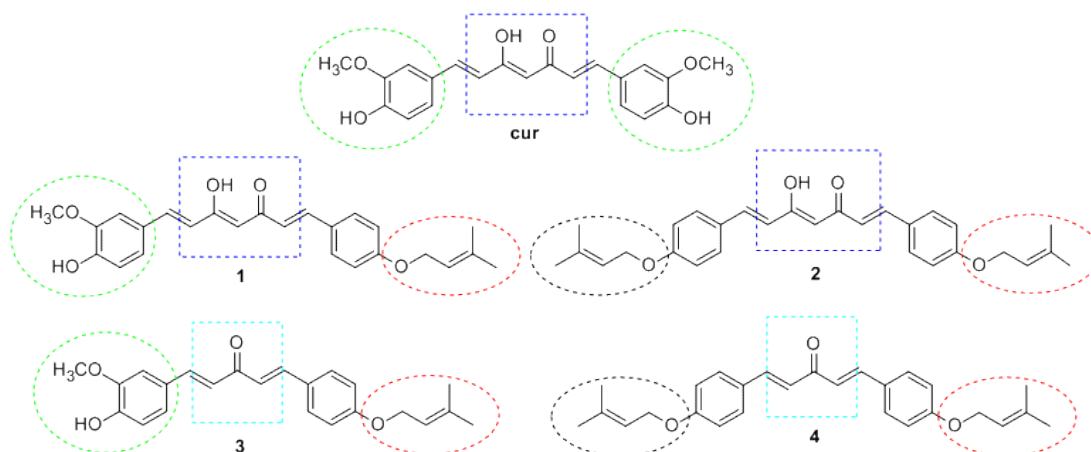
Figure 1. Design strategy toward the curcumin-based analogues **1-4.** Structures of curcumin (**cur**), the newly synthesized curcuminoids (**1, 2**) and their monocarbonyl analogues (**3, 4**).

Chemistry. The synthetic route for the attainment of the target curcumin-based compounds (**1-4**) is outlined in Schemes 1 and 2. Compounds **1** and **2** were prepared by two-consecutive steps, applying the Pabon reaction [28, 32]. Analogues **3** and **4** were synthesized through base-catalyzed Claisen-Schmidt procedure. In the classical Pabon procedure pentane-2,4-dione was complexed with B_2O_3 in EtOAc to avoid the methylene-centred reactivity toward the Knoevenagel reaction and to favor the nucleophilic attack at the side methyl groups. The boric complex was then condensed with the suitable aldehyde and then a step-

5

wise addition of *n*-tributylborate and *n*-butylamine was carried out. Acidic treatment caused the dissociation of the complex, providing the desired curcumin-based analogue. This reaction has been reported to give the curcuminoid as β-keto-enol tautomer. In the classical Claisen-Schmidt aldol condensation, acetone was reacted with the appropriate aldehyde in EtOH and in the presence of a 50% KOH/H$_2$O solution. In details, by condensing pentane-2,4-dione or acetone with two different selected aldehydes, namely 4-hydroxy-3-methoxybenzaldehyde (vanillin) and 4-(3,3-dimethylallyloxy)benzaldehyde, a mixture of the desired compounds could be obtained, among which the asymmetrical and the two symmetrical curcuminoids, including the semi-reaction products. Consequently, obtaining the desired compounds in a good purity grade would require several chromatographic purifications. To avoid this drawback, the synthesis of asymmetric curcumin analogues **1** and **3** (Scheme 1) was performed through two sequential steps, in which the semi-synthetic intermediates were first prepared reacting pentane-2,4-dione and acetone with vanillin under the appropriate reaction condition to give **5** and **6**, respectively. Subsequently, a second reaction with 4-(3,3-dimethylallyloxy)benzaldehyde, allowed the attainment of the desired asymmetrical compounds. In order to prepare the symmetrical analogues **2** and **4** (Scheme 2) a one-pot procedure, by using a 1:2 stoichiometric ratio for the ketone and the benzaldehyde, was performed. The 4-(3,3-dimethylallyloxy)benzaldehyde (**7**) was obtained by exploiting a Williamson ether synthesis between 4-hydroxybenzaldehyde and 3,3-dimethylallylbromide in the presence of K$_2$CO$_3$ as base.
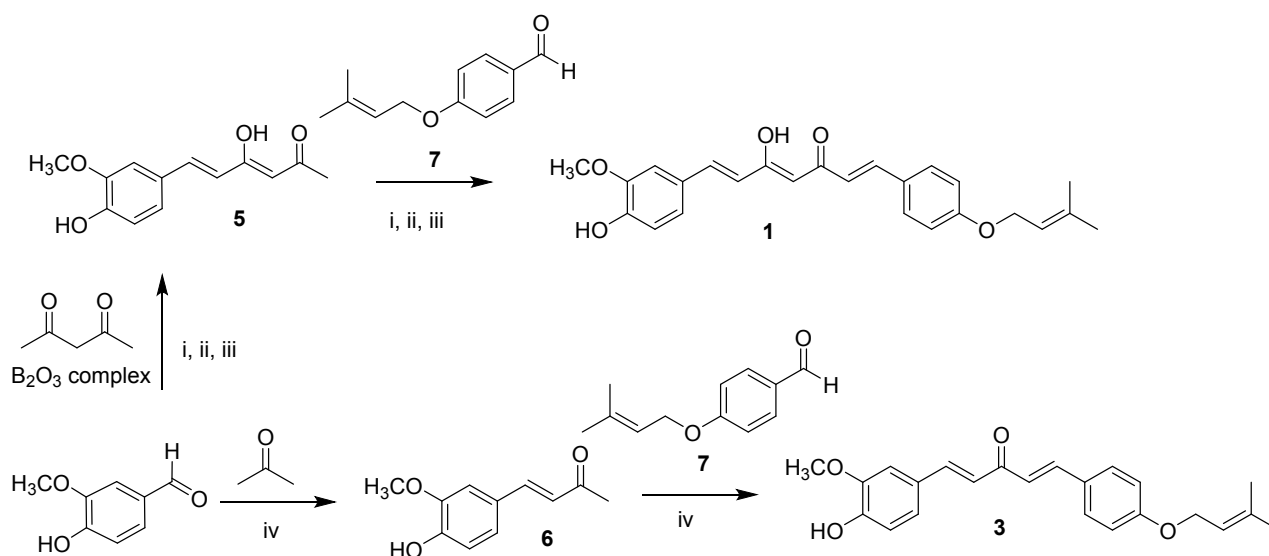
Scheme 1. Reagents and conditions: i) B(*n*-BuO)$_3$; ii) *n*-BuNH$_2$, 80 °C; iii) HCl, 80 °C; iv) KOH 50%. EtOH, rt.
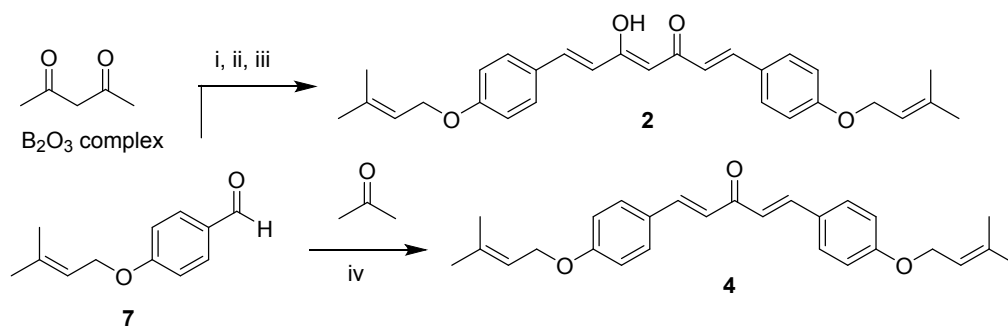
Scheme 2. Reagents and conditions: i) B(*n*-BuO)$_3$; ii) *n*-BuNH$_2$, 80 °C; iii) HCl, 80 °C; iv) KOH 50%. EtOH, rt.

Cell toxicity of curcumin and analogues. In view of evaluating if the Aβ$_{42}$ oligomers-induced toxicity is ameliorated in presence of the newly synthesized analogues (**1-4**), the intrinsic toxicity was assessed on neuroblastoma (SH-SY5Y) and microglia cells by using **cur** as reference compound. Cells were exposed to compound concentrations ranging from 1 to 50 µM for 24 hours or from 1 to 40 µM for 16 hours, respectively. As shown in Figure S1a), high concentrations (20-50 µM) of all tested compounds induced a significant loss of neuroblastoma cell viability in comparison to cells exposed to culture medium only. The di-prenoxylated derivatives **2** and **4** showed a significant and comparable profile, as toxic effects were observed at 5 µM concentration. At high concentrations (20-50 µM), **3** considerably reduced cell viability, conversely, at concentrations ranging from 1-10 µM it was found to be not toxic, alike **cur** and **1**.

Compound **2** exerted a similar effect on microglia cell viability, showing a cytotoxic activity from 1 µM concentration. Interestingly, treatment of microglia with **1**, even at 20 and 40 µM concentrations, did not significantly affect cell viability in comparison with vehicle-treated control cells, whereas the same concentrations of **cur** were cytotoxic (Figure S1b)), confirming previously published results [33].

Inhibition of Aβ$_{42}$ aggregation. On the basis of the amyloid hypothesis, a variety of anti-amyloid agents have been developed over the years, with the aim of interfering either with Aβ peptides oligomerization or fibrillogenesis or with both events [2, 14]. Despite the efforts made, results are not yet encouraging. The assays employed in *in vitro* aggregation studies show limitations in providing simultaneous and comparable information on both fibrils and oligomers, as well as among oligomers of different size. As a consequence, it is clear that more than one technique has to be used, since a potential inhibitor of the oligomerization may not be identified by using a specific assay for fibrils [14].

The evidence of fibril formation or inhibition is commonly given by well established techniques, such as transmission electron microscopy (TEM) and thioflavin T (ThT) fluorescence. Conversely, the identification and characterization of soluble Aβ oligomers involved in the pathological cascade are extremely challenging; indeed to date, a specific oligomeric state to target is missing [2, 14]. In particular, the difficulties

7

in obtaining well characterized Aβ oligomers in solution, as well as the dynamic equilibrium among oligomers which keep on aggregating during the *in vitro* experiments, represent important issues in the search for modulators of fibrillogenesis [34].

In this context, it has been demonstrated that capillary electrophoresis (CE) can play an alternative role in the *in vitro* aggregation studies of Aβ peptides. Since it works in free solution and in the absence of secondary equilibria, CE allows a real snapshot of Aβ while assembling into soluble oligomers inside the capillary, until sample precipitation [35]. The use of CE to identify agents able to interfere with Aβ$_{42}$ oligomerization has been pioneered by us and also reported by others [36-38]. Furthermore, the combination of CE analysis of Aβ$_{42}$ solutions in the presence of an anti-aggregating candidate with the TEM images of the final precipitate, provides integrated information on the anti-oligomerization and anti-fibrillogenesis activity [34-37].

Anti-oligomeric activity. In this work, we exploited one of the analytical platforms recently reported by us that were optimized and standardized to correlate aggregation state, structure and toxicity of Aβ$_{42}$ oligomers separated by CE, in view of coincubation experiments [34].

Before carrying out any analysis of an Aβ$_{42}$ sample in the presence of an inhibitor of aggregation, the setup of a reproducible protocol for Aβ$_{42}$ sample preparation and in turn of a reproducible CE separation of the prepared oligomers are mandatory prerequisites. Aβ$_{42}$ peptide aggregates and precipitates very rapidly, therefore to appreciate differences in oligomer formation kinetics or to detect reduction/abrogation of oligomer building-up by a coincubated compound, it is necessary to keep the assemblies in solution for a suitable time window. Moreover, the toxicity of the oligomeric populations detected and separated by CE has to be known, for identifying the target species of the small molecules evaluated.

In particular, for observing the effect of coincubated molecules, the least aggregating sample preparation protocol was selected [39], as it allows a wider time window if compared with other methods [36-38]. Since **cur** and compounds **1-4** are soluble in pure ethanol, an adjustment of the original Aβ$_{42}$ sample preparation protocol was necessary (see Experimental Section), to account for the percentage of ethanol in buffer when coincubating the peptide and the compounds. The comparison of the CE profile and mobility values reported in [34] with those of Aβ$_{42}$ control (i.e. in the absence of compounds) shown in Figure 2a) and Table S1 (Supplementary material), demonstrate that the kinetics of formation of oligomers and all electrophoretic parameters are not affected by a concentration of ethanol in buffer as high as 3.26%. Therefore, precise peak identification, molecular weight range and toxicity of the separated oligomers can be considered the same. Briefly, Figure 2a) shows the analysis of Aβ$_{42}$ peptide injected in the CE system after different elapsed times from sample solubilization (t0): monomers and dimers (peaks 1 and 2) progressively convert over time into neurotoxic aggregates larger than dodecamers (peak 3) [34]. At late times from solubilization, large aggregates are the most abundant species, until insoluble fibrils are formed

and no more soluble species are detected. As small oligomers are not toxic [34], a compound is considered active if it interferes with the formation of the assemblies migrating under peak 3.

All coincubation studies were carried out in triplicate and electrophoretic traces were recorded for **cur** and all analogues, at different concentrations and at different elapsed times from sample redissolution.

Figure 2b) shows the effect on the normalized area percentage of peak 3 in the presence of a given compound at the highest concentration tested (50 µM), at a time point where, for the control sample, the formation of toxic species is maximized (first bar). All compounds show some activity, although it is clear that the asymmetrical hepta-1,4,6-trien-3-one-based analogue **1** turns out to be the most effective of the series in suppressing the building up of toxic oligomers, followed by **cur** and then **2**, while the 1,4-dien-3-one analogues **3** and **4** are remarkably less active. Complete information on many time points from solubilization up to precipitation is reported in Figure S2, to appreciate how **1**, even at later times, is evidently more potent than **cur**.

Based on these results, experiments have been performed at 10 µM compound concentration, focusing the attention on **cur**, **1** and **2**, both endowed with the curcuminoid scaffold. Figure S3 (as compared to Figure 2 b)) shows how the activity is kept, in the same order, albeit with decreasing potency. Electropherograms in Figures 2 c) d) and e) easily visualize how derivative **1** (red trace) is best in suppressing the formation of large toxic oligomers (peak 3). The lower anti-aggregation activity of compound **2** (blue trace) could be partially ascribed at the lack of aromatic substituents capable of taking part in hydrogen bonding, which, conversely, are highly conserved in most amyloid ligands of natural origin [23].

Figure 2. Oligomerization of 100 µM Aβ$_{42}$ in the absence or in the presence of **cur** and of compounds **1-4**. a) Electrophoretic profiles of Aβ$_{42}$ control (solubilized in 3.26% EtOH in 20 mM phosphate buffer pH 7.4, see Experimental section) at selected elapsed times from t0 until precipitation: monitoring over time by CE. b) Anti-aggregation activity of 50 µM **cur** and compounds **1-4**: normalized area % of peak 3 at 21 days from sample redissolution as observed in control peptide and in the presence of compounds. Data are expressed as mean ± standard deviation, for n=3. c-e) Comparison between electrophoretic profiles of 100 µM Aβ$_{42}$ control (black trace) and in the presence of 10 µM **cur** (green traces), **1** (red traces) and **2** (blue traces) at different elapsed times from redissolution. Electropherograms are representative of n=3.

Complete evaluation at decreasing concentrations down to 1 µM is reported in Figure 3. Here the observations on the reduction of the toxic large oligomers (peak 3) can be summarized as follows: i) independently on the concentration tested, the symmetrical analogue **2** only slows down the formation of toxic oligomers, that are eventually formed as abundant as they are in the control sample; ii) both **cur** and **1** show concentration-dependent activity down to 1 µM (see also Figure S3); iii) at the lowest concentration and in comparison with **cur**, not only does **1** show a more consistent reduction (nearly double) of the toxic oligomers at the end point of the analyses, but it also keeps their abundance constantly low over time.
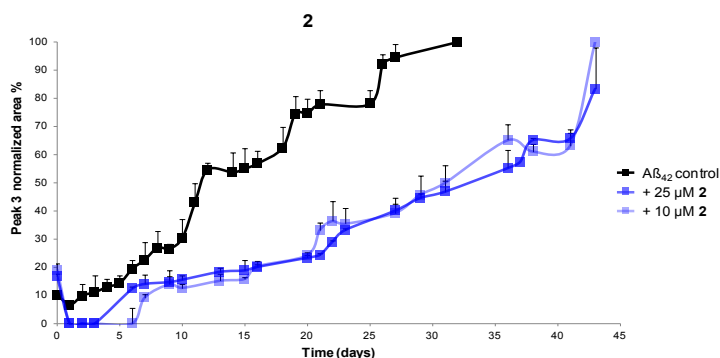
a)
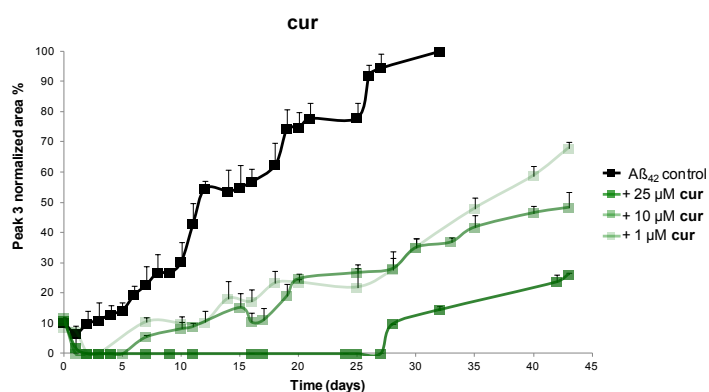
b)
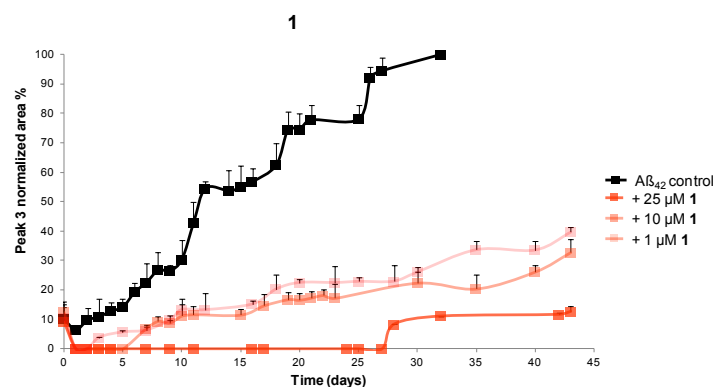
c)

Figure 3. Anti-oligomeric effect of compounds on toxic large oligomers (peak 3) over time. Normalized area percentage plot of peak 3 of 100 μM Aβ$_{42}$ control and in the presence of decreasing concentrations of: a) **cur**, b) **1**, c) **2**. Data are expressed as mean± standard deviation, for n=3.

Figure 2e) also provides information on the effect that coincubation of compounds exerts on the persistence in solution of non toxic monomers and dimers (earlier migrating peaks 1 and 2). In particular, it is clear that dimers (peak 2) are always kept in solution for very long times, in comparison with Aβ$_{42}$ control sample. This effect is consistent with the stabilization of Aβ dimers induced by curcumin [20]. Notably, from Figure S4, where the trend of the normalized area of dimers over time is reported, it can be derived that this effect is markedly induced by **cur** and by its mono 4-prenyloxy-aryl substituted **1,** in a concentration-dependent manner.

It can be summarized that CE data are consistent with the activity expected by virtue of the progressive structural modifications performed on **1**. In particular, the further substitution of the 4-hydroxy,3-methoxy group with the 4-prenyloxy (as for **2**) and the simplification of the β-keto enol function (as for **3**) result in a gradual decrease of the anti-oligomeric activity, that is lowest for **4,** in which both modifications are combined. The order of potency observed is **1>cur>2>3>4**.

Anti-fibrillogenic activity. Because of the intrinsic fluorescence of curcumin, ThT fluorescence assay is precluded [40], therefore TEM has been here employed to appreciate the effect of **cur** and **1**-**4** on fibril formation, fibril morphology and fibril density. Conclusions are drawn on data obtained for three independent samples each one measured in duplicate.

As shown in Figure 4, Aβ$_{42}$ peptide alone contains fibrils already at early stages from solubilization (24 hours), although, as explained in [34], these are not injected in the capillary of the CE system. Conversely to the control peptide and already after 24 hours, Aβ$_{42}$ samples coincubated with **cur** or **1** contain amorphous aggregates only. The absence of amyloid fibrils is kept at later stages of oligomerization (after 21 days). This evidence can be correlated with the anti-oligomeric activity induced by both compounds relative to large oligomers (Figure S2, 21 days) and consistently with the persistence in solution of dimers (Figure 2 e)).

The sample containing **cur** eventually precipitates into dense amyloid fibrils. This is not overly surprising, as also recent reports suggested that curcumin only inhibits oligomerization while promoting fibrillization [41, 42]; despite a growing evidence on the anti-amyloid effect of curcumin, the exact mechanism of action is still debated.

Contrary to samples coincubated with **cur**, only sporadic fibrils are detected in precipitated samples of Aβ$_{42}$ in the presence of derivative **1**. Surprisingly, compound **2** abrogates the formation of the fibrils observed after 24 hours, as only amorphous granular assemblies are detected at sample precipitation. In accordance with the poor anti-oligomeric activity, both monocarbonyl derivatives (**3** and **4**) lead to amyloid fibrils already after 24 hours and as end products of the aggregation (Figure 4).
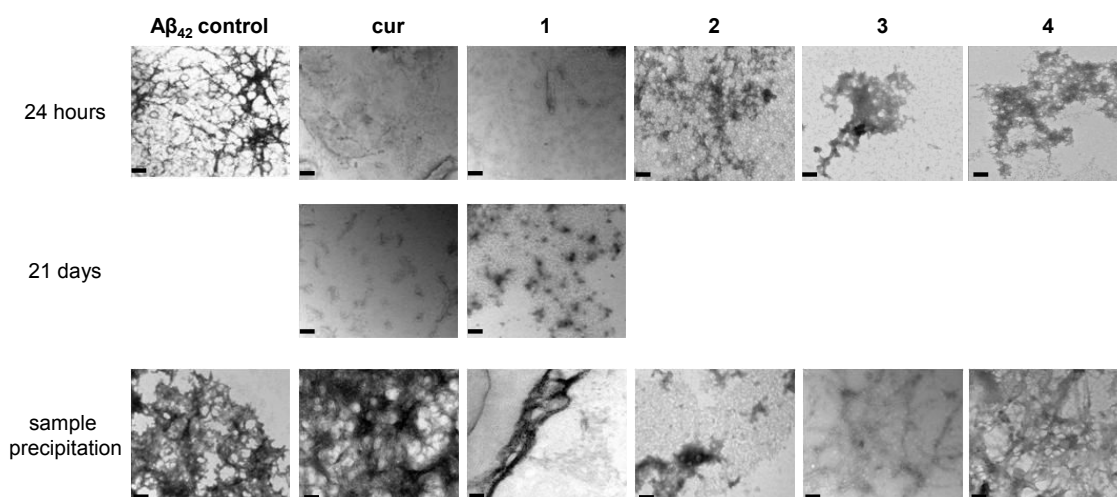
Figure 4. TEM images of Aβ$_{42}$ control peptide (100 μM) and 100 μM Aβ$_{42}$ coincubated with 50 μM **cur** and **1-4** analyzed at different times from redissolution. Scale bar=100nm. 60000x. n=3.
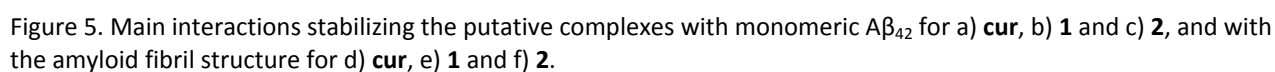
Modeling studies. Docking simulations were carried out to corroborate the effects of the curcumin-based analogues on Aβ$_{42}$ aggregation process and to elucidate by which specific interactions with Aβ residues the tested compounds are able to modify it. Even though the Aβ$_{42}$ peptide shows a marked flexibility and can assume almost all secondary motifs, docking simulations were focused on the peptide in its alpha-helix form because this is the only available resolved structure.

Figures 5 a) b) and c) show the best complexes obtained for **cur**, **1** and **2** with the monomeric Aβ$_{42}$ peptide. As expected, the ligands approach the amyloid region corresponding to the above mentioned [16]KLVFFA[21] sequence which is well-known to be involved in ligand recognition. In the computed complexes, the curcumin analogues assume slightly bent conformations which are in line with the curcumin geometries found in the resolved structures. For instance, the curcumin molecule included in the resolved complex with human transthyretin (PDB Id: 4PMF) shows an angle, as defined by the central carbonyl and the two aromatic rings, of 107.87 while, in the here generated complex, the same angle of **cur** is equal to 106.99 (see Figure 5a). Moreover and in all considered complexes, the β-keto-enol central core elicits H-bonds with Glu[22] and Ser[26], while a ligand phenyl ring stabilizes a clear π-π stacking contact with Phe[19]. The other interactions stabilized by the phenyl moieties depend on the polarity of the substituents. Thus, **cur**, through a side vanillin group, elicits H-bonds with Gln[15] and Asn[27], while asymmetrical analogue **1** retains the same polar contacts and, through its prenyloxy function, adds clear hydrophobic interactions with Ile[31]. The di-prenoxylated **2** loses the H-bond with Gln[15] and adds apolar contacts with Val[18]. Both monocarbonyl analogues (**3** and **4**) lose the key polar interactions with Glu[22] (complexes not shown). As depicted in Figure S5, the complexes as computed by considering more extended amyloid structures show comparable ligand poses even though the involvement of more amyloid segments increases the number of interacting residues especially concerning the hydrophobic residues.

While contacting the same well-known amyloid region, Figure 5 d) e) and f) show that the simulated ligands assume different poses when interacting with the fibril structures. In particular, the ligands assume rather extended geometries by which they contact six different amyloid segments. As seen for **1**, the ligands contact the same residues of all involved segments: in detail, they elicit i) extended hydrophobic contacts with six Leu[18] residues which contact both phenyl ring and alkyl chains and ii) extended H-bonds with six Lys[16] residues, which approach both the β-keto-enol central core and the substituents on phenyl rings. Not to mention that these protonated residues can also stabilize charge-transfer interactions with the phenyl rings. Taken together, one may observe that, while the ligands assume comparable poses in all simulated amyloid structures, the relevance of hydrophobic contacts increases when increasing the complexity of the simulated amyloid structure and finds its maximum expression with the fibril structure where the ligands are supported by a basis completely composed of apolar residues. These observations suggest that the interaction with simple amyloid structures are enhanced by a fine balance between polar and apolar contacts as seen for **1** in the monomeric protein, while the interaction with complex amyloid structures appears to be strongly governed by hydrophobic contacts.

The described molecular docking results find encouraging validations by SMD simulations involving $A\beta_{42}$ tetramers and fibrils and comparing **1** and **2** with **cur**. In these simulations the ligand is forced to unbound from the $A\beta_{42}$ structures and the required pulling force is monitored during the time. As compiled in Table S2, each simulated ligand is thus characterized by the time required to unbound the ligand (i.e. until the monitored force is 0 pN) as well as by the force mean required for unbinding. A third relevant parameter is the AUC value of the plot limited to the residence time which accounts for both the total force and required time. With regards to $A\beta_{42}$ tetramers, Table S2 shows that the most polar **cur** compound requires an initial marked force to break its key polar interactions (as reflected in the highest force mean) but then is unable to prolong its binding and indeed it shows a residence time and AUC values clearly lower than **1** and **2**. These results confirm that only a proper balance between polar and hydrophobic interactions is able to increase the stability of the complex with $A\beta_{42}$ oligomers over the time. In contrast and when simulating the fibrils, the ligands reveal rather similar values in all reported parameters. This observation may indicate that the ligands are here similarly governed by the sole hydrophobic contacts and indeed the most apolar compound (**2**) shows the best force mean and AUC value.

All proposed compounds were submitted to SwissADME online web-server (http://www.swissadme.ch) and resulted completely devoid of PAINS alerts with a predicted pharmacokinetic profile roughly comparable with that of the parent compound (results not shown).

14

Figure 5. Main interactions stabilizing the putative complexes with monomeric Aβ₄₂ for a) **cur**, b) **1** and c) **2**, and with the amyloid fibril structure for d) **cur**, e) **1** and f) **2**.

Evaluation of anti-inflammatory properties. The prenylation of aromatic natural products results in derivatives with an improved pharmacological profile when compared with not-prenylated compounds and prenylated natural compounds proved to be useful for the treatment of cancer and inflammation [29]. As this latter represents an important pathological condition in AD [3, 4], the functionalization of **cur** by the introduction of a prenyl function could enhance the anti-inflammatory potential.

Thus, the most promising compound **1** in terms of anti-oligomeric and anti-fibrillogenic activity, was selected to be tested for its anti-inflammatory properties, in comparison to **cur.** Lipopolysaccharide (LPS) is the major component of the outer membrane of gram-negative bacteria and a potent immune activator of a variety of mammalian cell types, including microglia. Inhibition of LPS-induced release of the pro-inflammatory cytokines IL-1β and TNF-α by microglia was examined to assess the anti-inflammatory effects of analogue **1** and **cur**. Microglia cells were exposed to non-cytotoxic concentrations of test compounds for 1 hour and then stimulated with LPS for 16 hours to induce an inflammatory response. In unstimulated cells low or undetectable amounts of IL-1β and TNF-α were released and these basal levels remained unchanged after treatment with the tested compounds (white bars, Figure 6). As expected, LPS stimulation induced an increased release of IL-1β and TNF-α (taken as 100%). Not only was this effect significantly suppressed by

15

cur, as we previously showed [33, 43], but also by its prenylated analogue **1,** starting from the concentration of 5 μM.
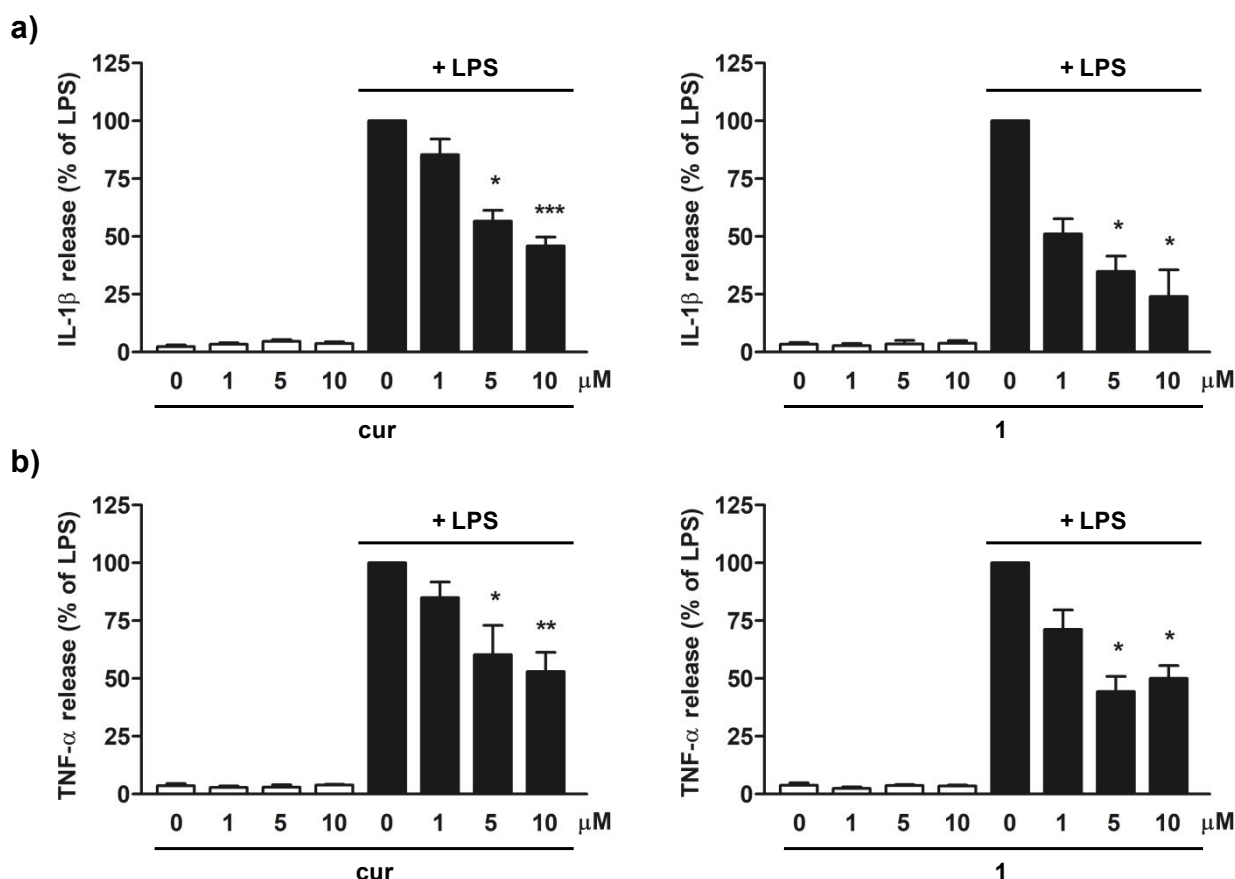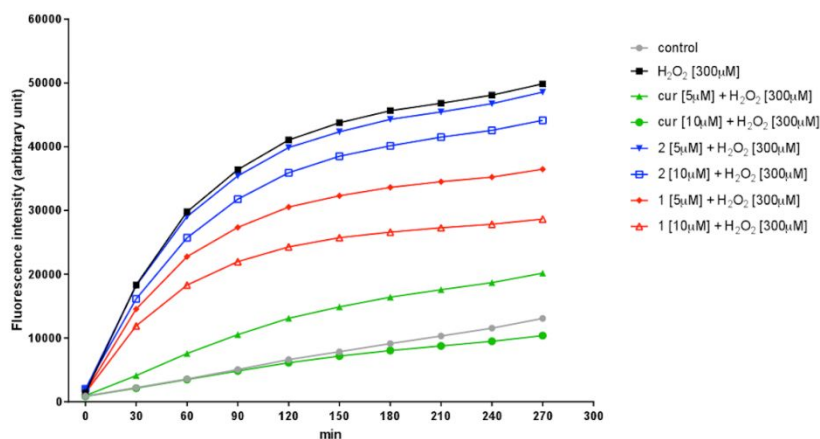

Figure 6. Effects of **cur** and analogue **1** on cytokine release from LPS-stimulated cortical microglia cells. a) IL-1β and b) TNF-α release. Data are mean ± SEM (standard error of mean) (n=3). * p<0.05, ** p<0.01 and *** p<0.001 *vs* LPS-stimulated cultures, Kruskal-Wallis followed by *post-hoc* Dunn's test.

Evaluation of anti-oxidant properties. In addition to the anti-inflammatory activity, we then investigated the potential of compounds **1** and **2** as antioxidants. We evaluated in SH-SY5Y neuroblastoma cells their scavenger ability when co-incubated with H_2O_2, using **cur** as reference. In comparison to untreated cells, (grey line, Figure 7a)), the intracellular DCFH-fluorescence intensity in H_2O_2-treated cells significantly increased (black line, Figure 7a)). Treatment with **cur** and compounds **1** and **2** reduced H_2O_2-induced intracellular ROS production, albeit to a different extent. At any time tested, **cur** showed the strongest scavenger activity when compared to analogues **1** and **2**. In particular, the presence of both vanillin moieties (as for **cur**) appears to be important for this anti-oxidant activity. Compound **2**, lacking 4-hydroxy,3-methoxy group on both aromatic rings, was less effective than compound **1**, where one of the two vanillin functions of curcumin is preserved.

16

Further studies were carried out on the mechanism of action of **1** and **2** on the Nrf2 cellular pathway, for investigating their ability to modulate the expression of the Nrf2 transcription factor [44]. Recent evidence further showed that Nrf2 activation suppresses inflammation through redox control [45]. Therefore, we investigated the activation of Nrf2 pathway by analyzing its translocation into nucleus. A concentration of 5 µM of **cur** and **1** induced Nrf2 nuclear translocation, whereas **2** did not show to be an Nrf2-inducer. The asymmetrical analogue **1**, at the concentration of 10 µM, did not produce statistically significant results in our experimental setting, although we could assume an increasing trend as compared to control (Figure 7 b)).

These data suggest that **1** may modulate anti-oxidant response by acting through different pathways, besides Nrf2 activation. Evidence from literature supports the ability of different natural products, including polyphenols in general, to interact with selected miRNAs, thus targeting multiple genes and showing pleiotropic activity [46]. Hence, the differential Nrf2 activation by 10 µM **1** may be putatively related to the modulation of the levels of certain miRNAs associated with the Nrf2 signaling pathway. On the basis of these observations, the investigation of miRNA modulation could potentially be important and will be next further evaluated to better understand the underlying anti-oxidant mechanism of natural products and their derivatives.
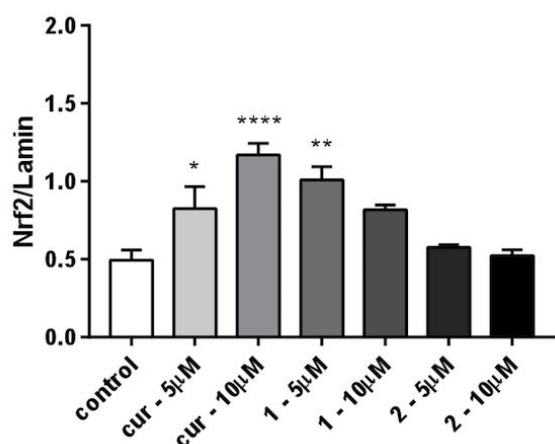
a)

b)

Figure 7. Anti-oxidant activity of **cur** and analogues **1** and **2**. a) Reduction of H_2O_2-induced intracellular ROS production: fluorescence intensity for all compounds is significant at any time from 30 to 270 min with $p<0.001$ vs H_2O_2, with exception of compound **2** at the concentration of 5 μM. For compound **2** the significance is as follows: $p<0.05$ at 90 min; $p<0.01$ at 120 min and 270 min; $p<0.001$ at 150, 180, 210 and 240 min. Dunnett's multiple comparison test; b) Activation of Nrf2 pathway: SH-SY5H cells were treated for 3 hours with compounds. Results are shown as ratio Nrf2/lamin ± SEM; *$p < 0.05$, **$p < 0.01$, ****$p<0.0001$ versus control; Dunnett's multiple comparison test.

CONCLUSIONS

The curcumin scaffold was rationally modified and a small set of structurally related compounds was obtained and tested against $A\beta_{42}$ oligomer and fibril formation, inflammation and oxidative stress, i.e. copathogenic factors related to AD. To this aim, derivatives were obtained in which i) a prenyloxy function was introduced as substituent in one or both the **cur** side aryl functions, and ii) the **cur** keto-enol central linker was simplified. Two couples of analogues **1**-**2**, and **3-4**, respectively were obtained.

The new compounds were firstly evaluated for their anti-amyloid effects, leading to identify **cur** and analogue **1**, both endowed with the hepta-trien-3-one linker, as the most effective agents in slowing down the formation of toxic Aβ oligomers. Interestingly, CE and TEM analyses showed how **1** potently inhibits oligomers building up and, contrary to **cur**, it does not lead to the formation of a dense network of fibrils. Due to its remarkably lower toxicity on microglia cells if compared to **2** and even to **cur**, analogue **1** was then selected to investigate its anti-inflammatory effect on microglia activation. In particular, at 5 μM concentration, a suppression of pro-inflammatory cytokines release was detected. This analogue also showed an anti-oxidant potential, with particular reference to the capability to induce, at 5 μM, Nrf2 nuclear translocation. By contrast, the symmetrical curcuminoid **2**, in comparison to **1**, showed a remarkably weaker anti-oxidant activity and a lower efficacy in contrasting oligomer formation. Notably, fibrils were not observed in presence of compound **2** and this suggests that the two prenyloxy substituents may serve as β-sheet breakers by intercalating in the amyloid fibrillar core. The anti-amyloid effects of **1** and **2**, compared to those of **cur**, were evidently corroborated by molecular docking and SMD simulations

18

which revealed the growing role of the hydrophobic interactions when simulating Aβ structures of increasing complexity. The simplified counterparts **3** and **4** failed to block both the formation of large Aβ assemblies and the deposition of fibrils.

Taken together, these data underlined the pivotal role of the curcumin scaffold in eliciting anti-amilodogenic effects, in particular when both the 4-hydroxy,3-methoxy and prenyloxy aryl substitution patterns are present. Indeed, among the newly synthesized compounds, **1** turned out to be a very promising anti-AD tool, endowed with a better biological profile with respect to **cur**. Due to its multipotent behaviour it could be a lead compound, worthy further optimization to obtain effective AD-modifying drug candidates.

EXPERIMENTAL SECTION

Chemicals and Materials. Synthetic $A\beta_{42}$ was purchased from Bachem (Bubendorf, Switzerland) as lyophilized powder and stored at -20°C. 1,1,1,3,3,3-Hexafluoropropan-2-ol (HFIP), acetonitrile (ACN), dimethylsulfoxide (DMSO) and sodium carbonate (Na_2CO_3) were from Sigma-Aldrich (St. Louis, MO, USA). Ethanol 96° was supplied by Carlo Erba (Cornaredo, Italy). Sodium hydroxide (NaOH) and sodium dodecyl sulphate (SDS) were provided by Merck (Darmstadt, Germany). Na_2HPO_4 and NaH_2PO_4, supplied by Sigma-Aldrich, were used for the preparation of the background electrolyte (BGE) in the CE analyses. BGE solutions were prepared daily using Millipore Direct-Q™ deionized water (Bedford, MA, USA) and filtered on 0.45 μm Sartorius membrane filters (Göttingen, Germany). Uncoated fused-silica capillary was from Polymicro Technologies (Phoenix, AZ, USA).

All cell culture reagents, culture medium and chemicals were purchased from Sigma-Aldrich.

Curcumin was purchased from Sigma Aldrich (analytical standard, purity ≥98%).

All samples containing curcumin and curcumin-derivatives were kept protected from light throughout all experiments.

Chemistry. General Procedures. Starting materials, unless otherwise specified in the Experimental Section, were used as high-grade commercial products. Solvents were of analytical grade. Melting points were determined in open glass capillaries, using a Büchi apparatus and are uncorrected. ^{1}H-NMR and ^{13}C-NMR spectra were recorded on Varian INOVA spectrometer operating at 400 MHz. Chemical shifts are reported as parts per million (ppm δ value). Standard abbreviations indicating spin multiplicities are given as follows: s (singlet), d (doublet), dd (doublet of doublet), t (triplet), br (broad), q (quartet) or m (multiplet). High-resolution mass spectra (HRMS) were acquired with an LTQ Orbitrap XL instrument (Thermo Fisher Scientific, Rodano, Milano. Resolution was set at 30000 (FWHM at 400 m/z) and scan range was 250-1000 m/z with a target of 5×10^5 ions per scan. Instrument control and data analysis/elaboration were provided

by the software Xcalibur (version 2.07, ThermoFisher Scientific, Rodano, MI, Italy). Chromatographic separations were performed on silica gel columns using the flash method (Kieselgel 40, 0.040-0.063 mm, Merck). Reactions were followed by thin layer chromatography (TLC) on precoated silica gel plates (Merck Silica Gel 60 F254) and then visualized with a UV lamp. Purities of all tested compounds used in the biological assays were determined by HPLC using the area percentage method on the UV trace recorded at 254 nm. The analyses were performed under reversed-phase conditions on a Phenomenex Luna 5μm C18 column (150 × 4.60 mm), by using a ternary mixture of 0.1 % H_3PO_4/MeCN/MeOH (40:40:20, v/v) as mobile phase, flow rate: 0.7 mL / min. A liquid chromatograph PU-1587 UV model equipped with a 20 μL loop valve (Jasco Europe, Italy) was employed. All compounds were found to have >95% purity, as confirmed by NMR spectra (see Supplementary material). Compounds were named using Chem-BioDraw Ultra 14.0 IUPAC name algorithm developed by CambridgeSoft Corporation.

4-(3,3-dimethylallyloxy)benzaldehyde (7). 4-hydroxybenzaldehyde (1.00 g, 8.19 mmol) and 3,3-dimethylallyl bromide (1.14 mL, 9.83 mmol) were allowed to react according to the general procedure of the Williamson reaction for 8 h to give the crude product that was purified by crystallization from PE; yellow oil, 83 % yield. ^{1}H-NMR (400 MHz, CDCl$_3$): δ 1.76 (s, 3H, CH$_3$), 1.81 (s, 3H, CH$_3$), 4.60 (d, 2H, J = 6.8 Hz, OCH$_2$), 5.45 (t, 1H, J = 6.8 Hz, CH=), 7.00 (d, 2H, J = 8.8 Hz, H-3' and H-5'), 7.83 (d, 2H, J = 8.8 Hz, H-2' and H-6'), 9.88 (s, 1H, CHO).

Pabon reaction: general procedure for the synthesis of compounds 1, 2, and 5. To a stirred solution of pentane-2,4-dione (1.00 mmol) in EtOAc (1.0 mL), B_2O_3 (1.0 molar equiv) was added, and the suspension was stirred for 30 min at 80 °C before addition of a solution of the appropriate aldehyde/s, (0.9 molar equiv for monoaryl or 1.8 molar equiv for bi-aryl curcumin derivatives), tri-n-butyl borate (2.0 molar equiv for monoaryl or 4.0 molar equiv for bi-aryl curcumin derivatives), in EtOAc (0.5 mL). The reaction mixture was stirred at 80 °C for 30 min, then a solution of n-butylammine (0.4 molar equiv in 1.0 mL of EtOAc) was added over a period of 15 min. The mixture was heated to 80 °C for 8 h and then, after cooling to r.t., it was acidified with 0.5 N HCl (30 mL) and then stirred at 80 °C for 30 min. The organic phase was separated and the aqueous layer was extracted with EtOAc (3 x 10 mL). The combined organic layers were sequentially washed with saturated aqueous NaHCO$_3$ and brine, dried over Na$_2$SO$_4$, filtered, and concentrated under reduced pressure. The crude residue was purified by flash column chromatography using a mixture of petroleum ether / ethyl acetate (PE / EtOAc) as eluent, followed by crystallization from suitable solvent.

3Z,5E-4-hydroxy-6-(4-hydroxy-3-methoxyphenyl)hexa-3,5-dien-2-one (5) [28]**.** Reaction of pentane-2,4-dione (0.50 g, 5.00 mmol), B_2O_3 (0.45 g, 5.00 mmol), and vanillin (0.69 g, 4.5 mmol), in EtOAc (7.5 mL), gave a crude product that was purified by flash chromatography (PE / EtOAc, 9.75:0.25), yellow powder, 55% yield, mp 144-146 °C (EtOH). ^{1}H NMR (400 MHz, CDCl$_3$): δ 2.16 (s, 3H, CH$_3$), 3.94 (s, 3H, OCH$_3$), 5.40 (br, 1H, OH),

5.63 (s, 1H, keto-enol-CH), 6.33 (d, J = 16.0 Hz, 1H, CH=CH), 6.92 (d, J = 8.0 Hz, 1H, H-5), 7.02 (d, J = 1.8 Hz, 1H, H-2), 7.09 (dd, J = 1.8, 8.0 Hz, 1H, H-6), 7.53 (d, J = 16.0 Hz, 1H, CH=CH).

(1E,4Z,6E)-5-hydroxy-7-(4-hydroxy-3-methoxyphenyl)-1-(4-((3-methylbut-2-en-1-yl)oxy)phenyl)hepta-1,4,6-trien-3-one (1). Reaction of intermediate **5** (0.23 g, 1.00 mmol) and **7** (0.17 g, 0.9 mmol) gave a crude product that was purified by flash chromatography (PE/EtOAc, 8.5:1.5) and further crystallization from EtOH affording **1** as orange solid, 41 % yield, mp 144-146 °C. ^{1}H-NMR (CDCl$_3$): δ 1.77 (s, 3H, CH$_3$), 1.82 (s, 3H, CH$_3$), 3.96 (s, 3H, OCH$_3$), 4.56 (d, J = 6.8 Hz, 2H, OCH$_2$), 5.50 (t, J = 6.8 Hz, 1H, CH=C), 5.80 (s, 1H, keto-enol-CH), 5.85 (br s, 1H, OH), 6.49 (d, J = 15.6 Hz, 1H, CH=CH), 6.50 (d, J = 15.6 Hz, 1H, CH=CH), 6.94 (d, J = 8.0 Hz, 2H, H-3'and H-5'), 6.95 (d, J = 8.0 Hz, 1H, H-5), 7.07 (s, 1H, H-2), 7.13 (d, J = 8.0 Hz, 1H, H-6), 7.51 (d, J = 8.8 Hz, 2H, H-2' and H-6'), 7.60 (d, J = 15.6 Hz, 1H, CH=CH), 7.63 (d, J = 15.6 Hz, 1H, CH=CH). ^{13}C-NMR (CDCl$_3$): δ 18.4, 26.0, 56.1, 65.1, 101.4, 109.7, 115.0, 115.2 (2C), 119.4, 122.0, 121.9, 123.1, 127.8, 127.9, 129.9 (2C), 138.9, 140.4, 140.6, 146.9, 148.0, 160.8, 183.4, 183.5. HRMS (ESI) calcd. for C$_{25}$H$_{27}$O$_5$ [14+] 407.18530; found 407.18533 (Δ = 0.1 ppm).

(1E,4Z,6E)-5-hydroxy-1,7-bis(4-((3-methylbut-2-en-1-yl)oxy)phenyl)hepta-1,4,6-trien-3-one (2). Reaction of pentane-2,4-dione (0.15 mL, 1.46 mmol) and **7** (0.5 g, 2.63 mmol) gave the crude product that was purified by flash chromatography (PE/EtOAc, 9.75:0.25) and further crystallization from EtOH, affording **2** as yellow solid, 45 % yield, mp 165-167 °C. ^{1}H-NMR (400 MHz, CDCl$_3$): δ 1.76 (s, 6H, CH$_3$), 1.81 (s, 6H, CH$_3$), 4.56 (d, J = 6.8 Hz, 4H, OCH$_2$), 5.50 (t, J = 6.8 Hz, 2H, CH=C), 5.78 (s, 1H, keto-enol-CH), 6.51 (d, J = 15.6 Hz, 2H, CH=CH), 6.93 (d, J = 8.4 Hz, 4H, H-3'and H-5'), 7.51 (d, J = 8.4 Hz, 4H, H-2' and H-6'), 7.63 (d, J = 15.6 Hz, 2H, CH=CH). ^{13}C-NMR (100 MHz, CDCl$_3$): δ 18.4 (2C), 26.0 (2C), 65.1 (2C), 101.5, 115.2 (4C), 119.4 (2C), 121.9 (2C), 127.9 (2C), 129.9 (4C), 138.8 (2C), 140.3 (2), 160.8 (2C), 183.5 (2C). HRMS (ESI) calcd. for C$_{29}$H$_{33}$O$_4$ [14+] 445.23734; found 445.23553 (Δ = −1.6 ppm).

Claisen–Schmidt Reaction: general procedure for the synthesis of compounds 3, 4, and 6. To a solution of ketone (1.0 mmol) and the selected aldehyde (1.1 mmol or 2.2 mmol) in EtOH (10 mL), a KOH aqueous solution (50% p/v, 1 mL) was added dropwise. The reaction mixture was stirred overnight at room temperature, then diluted with H$_2$O and acidified with aqueous 6N HCl. The separated solid was collected by *vacuum* filtration and purified by flash chromatography or by crystallization.

(E)-4-(4-hydroxy-3-methoxyphenyl)but-3-en-2-one (6). Reaction of propan-2-one (0.25 g, 5.00 mmol), vanillin (0.98 g, 5.5 mmol), in EtOH (5.0 mL), gave a crude product that was purified by crystallization from EtOH to give **6** as white solid, 75% yield, mp 95-98 °C. ^{1}H NMR (400 MHz, CDCl$_3$): δ 2.37 (s, 3H, CH$_3$), 3.94 (s, 3H, OCH$_3$), 5.99 (br, 1H, OH), 6.59 (d, J = 16.0 Hz, 1H, CH=CH), 6.94 (d, J = 8.4 Hz, 1H, H-6), 7.06 (d, J = 2.0 Hz, 1H, H-2), 7.09 (dd, J = 2.0, 8.4 Hz, 1H, H-5), 7.46 (d, J = 16.0 Hz, 1H, CH=CH).

(1E,4E)-1-(4-hydroxy-3-methoxyphenyl)-5-(4-((3-methylbut-2-en-1-yl)oxy)phenyl)penta-1,4-dien-3-one (3). Reaction of intermediate **6** (0.19 g, 1.00 mmol) and **7** (0.21 g, 1.1 mmol), gave the crude product that

was purified by flash chromatography (PE/EtOAc, 7:3) and further crystallization from EtOH, affording **3** as pale orange solid 85% yield, mp 101-113 °C. ^{1}H NMR (400 MHz, CDCl$_3$): δ 1.77 (s, 3H, CH$_3$), 1.82 (s, 3H, CH$_3$), 3.96 (s, 3H, OCH$_3$), 4.56 (d, J = 6.8 Hz, 2H, OCH$_2$), 5.50 (t, J = 6.8 Hz, 1H, CH=C), 5.97 (br, 1H, OH), 6.91-7.00 (m, 5H, CH=CH, H-5, H-3', H-5'), 7.12 (d, J = 1.6 Hz, 1H, H-2), 7.18 (dd, J = 2.0, 8.4 Hz, 1H, H-6), 7.57 (d, J = 8.8 Hz, 2H, H-2' and H-6'), 7.67 (d, J = 15.2 Hz, 1H, CH=CH), 7.71 (d, J = 15.2 Hz, 1H, CH=CH). ^{13}C NMR (100 MHz, CDCl$_3$): δ 18.4, 26.0, 56.1, 65.1, 109.9, 115.0, 115.2 (2C), 119.3, 123.2, 123.5, 123.8, 127.6, 130.2 (2C), 138.9, 142.9, 143.2, 147.0, 148.3, 161.1, 189.0. HRMS (ESI) calcd. for C$_{23}$H$_{25}$O$_4$ [14+] 365.17474; found 365.17471 (Δ = −0.1 ppm).

(1E,4E)-1,5-bis(4-((3-methylbut-2-en-1-yl)oxy)phenyl)penta-1,4-dien-3-one (4) [47]. Reaction of propan-2-one (0.25 g, 5.00 mmol), vanillin (1.95 g, 11.0 mmol), in EtOH (5.0 mL), gave a crude product that was purified by crystallization from EtOH to give **4** as yellow solid, 87% yield, mp 74-76 °C. ^{1}H NMR (400 MHz, CDCl$_3$): δ 1.77 (s, 6H, CH$_3$), 1.82 (s, 6H, CH$_3$), 4.56 (d, J = 6.8 Hz, 4H, OCH$_2$), 5.50 (t, J = 6.8 Hz, 2H, CH=C), 6.94-6.98 (m, 6H, CH=CH, H-3, H-5),7.56 (d, J = 8.8 Hz, 4H, H-2 and H-6), 7.70 (d, J = 16.0 Hz, 2H, CH=). ^{13}C NMR (CDCl$_3$) δ 18.3 (2C), 25.9 (2C), 65.0 (2C), 115.2 (4C), 119.3 (2C), 123.5 (2C), 127.6 (2C), 130.1 (4C), 138.8 (2C), 142.8 (2C), 161.0 (2C), 189.0. HRMS (ESI) calcd. for C$_{27}$H$_{31}$O$_3$ [14+] 403.22677; found 403.22675 (Δ = 0.0 ppm).

Capillary electrophoresis. Aβ_{42} peptide was solubilized by following the procedure described in [39]. Briefly, lyophilized Aβ_{42} was dissolved in HFIP and then the solvent was left to evaporate after an appropriate incubation time. The Aβ_{42} aliquots were redissolved in a basic mixture (ACN/300 µM Na$_2$CO$_3$/250 mM NaOH, 48.3:48.3:3.4, v/v/v) to obtain 500 µM Aβ_{42}. This solution was then diluted to the operative concentration (100 µM Aβ_{42} control peptide) with 20 mM phosphate buffer pH=7.4, with or without small molecules.

Stock solutions of **cur** and of curcumin-based analogues (1.53 mM) were prepared in pure ethanol.

For co-incubation studies, 500 µM Aβ_{42} peptide (in the basic mixture) was resuspended in an appropriately diluted compound solution, so as to keep the peptide concentration at 100 µM and obtain different peptide/compound ratios: 1:100, 1:10, 1:4, 1:2 for **cur** and **1**; 1:10, 1:4, 1:2 for **2** and 1:2 for **3** and **4**. The final percentage of ethanol was equal or lower than 3.26%.

The aggregation process of Aβ_{42} in the presence or not of **cur** and of curcumin-based analogues was monitored by an Agilent Technologies 3D CE system with built-in diode-array detector (Waldbronn, Germany), following the analytical method reported in [34]. For the separation, a fused silica capillary (Polymicro Technologies, Phoenix, AZ, USA) of 33 cm (24.5 cm, effective length) was employed. The background electrolyte (BGE, 80 mM Na$_2$HPO$_4$/NaH$_2$PO$_4$ (pH 7.4)) was prepared daily and filtered on 0.45 µm membrane filters.The injection of the samples was carried out by applying a pressure of 30 mbar for 3 s. The capillary was thermostatted with circulating air at 25°C and separations were carried out at 12 kV

(operative current: 75–78 µA) with the anode at the sample injection end. The acquisition wavelength was 200 nm. Oligomeric species were identified on the basis of effective mobilities (µeff), which are calculated by subtracting the contribute of the electrosmotic flow (µEOF) from the apparent mobility (µapp). Electrosmotic flow is measured as a perturbation of the baseline due to the sample solvent mixture. Semiquantitative analyses were performed based on the normalized area % [34].

Transmission Electron Microscopy. Amyloid fibril indentification was carried out by using a JEOL JEM 1400-Plus electron microscope (Peabody, MA, USA) operating at 80 kV. When no more peaks are detected by CE, precipitated samples were prepared as follows: $A\beta_{42}$ sample suspensions with or without **cur** and analogues **1-4** were diluted at 10 µM with 20 mM Na_2HPO_4/NaH_2PO_4 and then 10 µL of diluted suspensions were left to sediment on carbon-coated Formvar nickel grids (200 mesh) (Electron Microscopy Sciences, Washington, PA,USA). After 15 minutes the excess of sample was drained off by means of a filter paper. The negative staining was performed with 10 µL of 2%w/v uranyl acetate solution (Electron Microscopy Sciences).

Docking studies. In order to rationalize the different activity of curcumin and the here proposed derivatives, molecular docking simulations were performed involving the resolved $A\beta_{42}$ peptide (PDB Id: 1IYT), which was simulated in its monomeric, dimeric and tetrameric forms. Calculations also included the resolved amyloid fibril (PDB Id: 2MXU). The ligands were simulated in their keto-enolic form and their conformational space was explored by combining MonteCarlo simulations and PM7-based semi-empirical minimizations as previously described [48]. In detail, the amyloid monomer was minimized by keeping fixed the backbone atoms to preserve the resolved folding and utilized to build the corresponding dimer by following the computational procedure as described by Rao and co-workers [49]. Briefly, two optimized monomers were initially aligned at an average distance between the backbone atoms of the two monomers of about 10 Å and then the monomers were progressively approached and optimized to reach a final average distance of about 5 Å. The resolved fibril structure underwent the same refinement protocol as described for monomer before docking simulations. Thus, SMD simulations involved $A\beta_{42}$ in its monomeric, dimeric and fibril forms and were performed by using PLANTS and by including the entire amyloid structure in its searches [50]. For each simulated ligand, 20 poses were generated and ranked by ChemPLP score with a speed equal to 1. All obtained poses were then minimized. The best dimeric complexes were finally utilized to generate the corresponding tetramers by docking on them a second dimer structure. Such a dimer-dimer docking was performed using PatchDock by adopting its default parameters and the so generated 20 docking results were finally refined by FireDock [51]. The so produced best tetrameric complexes were finally minimized by keeping fixed the backbone atoms. The computed tetrameric and fibril complexes for **1**, **2** and **cur** were then neutralized and inserted into a 80 Å side box of

water. After a preliminary minimization, the systems underwent 3 ns SMD simulations with the same characteristics as described in [52].

Inhibition of cytokines release. All animal-related procedures complied with the ARRIVE guidelines and were performed in accordance with EU guidelines for the care and use of laboratory animals and those of the Italian Ministry of Health (D.Lg. 26/2014) and were approved by the Institutional Review Board for Animal Research (Organismo Preposto al Benessere Animale, OPBA) of the University of Padua and by the Italian Ministry of Health (Protocol number 958/2016-PR). One-day old Sprague-Dawley rat pups (CD strain) were rapidly decapitated, minimizing suffering, discomfort or stress. Primary microglia cells were isolated from mixed glial cell cultures prepared from cerebral cortex, as previously described [53]. Briefly, upon reaching confluence (7–10 days after isolation) microglia adhering to the astroglial monolayer were dislodged by shaking (200 r.p.m. for 1 h at 37°C), resuspended in high-glucose Dulbecco's Modified Eagle's Medium (DMEM) supplemented with 2 mM L-glutamine, 10% heat-inactivated fetal bovine serum (FBS), 100 U/mL penicillin, 100 μg/mL streptomycin and 50 μg/mL gentamicin and plated on uncoated plastic wells at a density of 1.25×10^5 cells/cm^2. Cells were allowed to adhere for 45 min and then washed to remove non-adhering cells. After a 24 h incubation period, the medium was replaced with serum-free medium containing the agents under study. Purity of the cultures was confirmed by immunocytochemistry using a primary polyclonal antibody against ionized calcium binding adaptor molecule 1 (Iba1, 1:800, Wako Chemicals USA Inc., Richmond, VA, USA). Ninety-seven per cent of the cells were Iba1 immunopositive. Cells were maintained at 37°C in a humidified atmosphere containing 5% CO_2/95% air.

Microglia were pre-treated for 1 hour with non-cytotoxic concentrations of **cur** and **1** and then stimulated with 100 ng/mL Ultra-Pure LPS-EB for an additional 16 hours. At the end of incubation, culture medium was collected and the levels of IL-1β and TNF-α released by microglia were assayed using a commercially available ELISA kits (Antigenix America, Huntington Station, NY, USA), according to the manufacturer's instructions. Cytokine concentrations (pg/mL) in the medium were determined by reference to standard curves obtained with known amounts of IL-1β and TNF-α and the results expressed as percentage relative to LPS-stimulated cultures. Data were analyzed using GraphPad software, version 3.03 (GraphPad Software, Inc., La Jolla, CA, USA) and expressed as mean ± SEM of at least 3 independent experiments. As raw values varied between experiments and the variability could obscure the treatment effect, data were expressed as percentage LPS treatment, taken as baseline of each independent experiment. Data were analyzed by means of Kruskal-Wallis one-way analysis of variance followed by post-hoc Dunn's test for multiple comparisons vs LPS treatment. Significance level was set at $p < 0.05$. Additional details are provided in the figure legends, where appropriate.

Measurement of intracellular ROS. The fluorescent probe 2,7-dichlorodihydrofluorescein diacetate (DCFH-DA) (Merck KGaA, Darmstadt, Germany) was used as a specific marker for quantitative intracellular

24

ROS formation. Cells (2x10^4 cells per well) were loaded with 25 µM DCFH-DA for 45 min. After centrifugation DCFH-DA was removed and cells were exposed to 5 and 10 µM of **cur**, compounds **1** and **2** and 300 µM H$_2$O$_2$. ROS levels were determined from 0 to 270 min using Synergy HT multidetection microplate reader (BioTek) with excitation and emission wavelengths of 485 and 530 nm, respectively.

Immunodetection of Nrf2. The expression of Nrf2 in nuclear cell lysates was assessed using Western blot analysis. Cell monolayers were washed twice with ice-cold PBS, harvested and subsequently homogenized 15 times using a glass-glass dounce homogenizer in ice-cold fractionation buffer (20 mM Tris/HCl pH 7.4, 2 mM EDTA, 0.5 mM EGTA, 0.32 M sucrose, 50 mM β-mercaptoethanol). The homogenate was centrifuged at 300×g for 5 min to obtain the nuclear fraction. An aliquot of the nuclear extract was used for protein quantification, whereas the remaining extract was prepared for Western blot by mixing the nuclear cell lysate with 2X sample buffer (125 mM Tris-HCl pH 6.8, 4% SDS, 20% glycerol, 6% β-mercaptoethanol, 0.1% bromophenol blue) and then denaturing at 95°C for 5 min. Equivalent amounts of nuclear extracted proteins were loaded into a SDS-PAGE gel, electrophoresed under reducing conditions, transferred to a PVDF membrane (Merck KGaA, Darmstadt Germany) and then blocked for 1 hour with 5% w/v BSA in Tris-buffered saline containing 0.1% Tween 20 (TBS-T). Membranes were immunoblotted with rabbit anti-human Nrf2 (1:2000) diluted in 5% w/v BSA in TBS-T. Detection was carried out by incubation with horseradish peroxidase conjugated goat anti-rabbit IgG (1:5000 dilution in 5% w/v BSA in TBS-T) for 1 hour at room temperature. Membranes were then washed three times with TBS-T and proteins of interest were visualized using an enhanced chemiluminescent reagent (Pierce, Rockford, IL, USA). Lamin A/C was performed as a control for gel loading.

SUPPORTING INFORMATION

Cell viability data, further capillary electrophoresis data, further molecular docking results and steered molecular dynamics data, ^{1}H NMR spectra, ^{13}C NMR spectra, 2D-COSY spectra.

ABBREVIATIONS

AD, Alzheimer's disease; Aβ, amyloid-beta; Aβ$_{42}$, Aβ$_{1-42}$; CE, capillary electrophoresis; AUC, area under the curve; DMSO, dimethylsulfoxide; cur, curcumin; HFIP, 1,1,1,3,3,3-Hexafluoropropan-2-ol; LPS, lipopolysaccharide; SMD, steered molecular dynamics; MTT, 3-(4,5-dimethylthiazol-2-ly)-2,5-diphenyltetrazolium bromide; ROS, reactive oxygen species; TEM, transmission electron microscopy;

AUTHOR INFORMATION

Corresponding author: Prof. Ersilia De Lorenzi, Department of Drug Sciences, University of Pavia, Viale Taramelli 12, 27100, Pavia, Italy; tel +39 0382 987747; fax +39 0382 422975; email ersidelo@unipv.it.

Author contributions: **E. De Lorenzi** conceived the project, supervised all contributions and finalized the draft manuscript. **F. Bisceglia** performed CE studies and data analysis, TEM data interpretation, figures and manuscript preparation. **F. Seghetti** synthesized curcumin analogues and performed NMR data. **M. Serra** assisted data analysis and interpretation, the revision of final version of the manuscript and NMR results. **M. Zusso** conceived and carried out the data on microglia, wrote the draft text and prepared the figures of the relative section. **S. Gervasoni** performed molecular modelling studies and assisted data discussion. **L. Verga** performed TEM data and elaborated the relative images. **G. Vistoli** conceived and supervised the molecular modelling studies and wrote the draft of the relative section. **C. Lanni** conceived and supervised the experiments on anti-oxidant activity and cell viability on neuroblastoma cells, wrote the draft of the relative section. **M. Catanzaro** carried out the cell viability experiments on neuroblastoma cells and the data on anti-oxidant activity. **F. Belluti** conceived the design of curcumin analogues, supervised synthesis and NMR characterization, drafted the manuscript.

The authors declare that none of them has competing financial interests in this work.

Conflict of interest: The authors declare that none of them has competing financial interests in this work.

ACKNOWLEDGEMENTS

26

REFERENCES

1. Winblad, B., Amouyel, P., Andrieu, S., Ballard, C., Brayne, C., Brodaty, H., Cedazo-Minguez, A., Dubois, B., Edvardsson, D., Feldman, H., Fratiglioni, L., Frisoni, G. B., Gauthier, S., Georges, J., Graff, C., Iqbal, K., Jessen, F., Johansson, G., Jonsson, L., Kivipelto, M., Knapp, M., Mangialasche, F., Melis, R., Nordberg, A., Rikkert, M. O., Qiu, C., Sakmar, T. P., Scheltens, P., Schneider, L. S., Sperling, R., Tjernberg, L. O., Waldemar, G., Wimo, A., and Zetterberg, H. (2016) Defeating Alzheimer's disease and other dementias: a priority for European science and society, *Lancet Neurol 15,* 455-532.

2. Chiti, F., and Dobson, C. M. (2017) Protein Misfolding, Amyloid Formation, and Human Disease: A Summary of Progress Over the Last Decade, *Annu Rev Biochem 86,* 35.1-35.42.

3. Calsolaro, V., and Edison, P. (2016) Neuroinflammation in Alzheimer's disease: Current evidence and future directions, *Alzheimers Dement 12,* 719-732.

4. Querfurth, H. W., and LaFerla, F. M. (2010) Alzheimer's disease, *N Engl J Med 362*, 329-344.

5. Younkin, S. G. (1995) Evidence that A beta 42 is the real culprit in Alzheimer's disease, *Ann Neurol 37*, 287-288.

6. Da Mesquita, S., Ferreira, A. C., Sousa, J. C., Correia-Neves, M., Sousa, N., and Marques, F. (2016) Insights on the pathophysiology of Alzheimer's disease: The crosstalk between amyloid pathology, neuroinflammation and the peripheral immune system, *Neurosci Biobehav Rev 68*, 547-562.

7. Maji, S. K., Ogorzalek Loo, R. R., Inayathullah, M., Spring, S. M., Vollers, S. S., Condron, M. M., Bitan, G., Loo, J. A., and Teplow, D. B. (2009) Amino acid position-specific contributions to amyloid beta-protein oligomerization, *J Biol Chem 284*, 23580-23591.

8. Liao, M. Q., Tzeng, Y. J., Chang, L. Y., Huang, H. B., Lin, T. H., Chyan, C. L., and Chen, Y. C. (2007) The correlation between neurotoxicity, aggregative ability and secondary structure studied by sequence truncated Abeta peptides, *FEBS Lett 581,* 1161-1165.

9. Tjernberg, L. O., Lilliehook, C., Callaway, D. J., Naslund, J., Hahne, S., Thyberg, J., Terenius, L., and Nordstedt, C. (1997) Controlling amyloid beta-peptide fibril formation with protease-stable ligands, *J Biol Chem 272*, 12601-12605.

10. Belluti, F., Rampa, A., Gobbi, S., and Bisi, A. (2013) Small-molecule inhibitors/modulators of amyloid-beta peptide aggregation and toxicity for the treatment of Alzheimer's disease: a patent review (2010 - 2012), *Expert Opin Ther Pat 23*, 581-596.

11. Cleary, J. P., Walsh, D. M., Hofmeister, J. J., Shankar, G. M., Kuskowski, M. A., Selkoe, D. J., and Ashe, K. H. (2005) Natural oligomers of the amyloid-beta protein specifically disrupt cognitive function, *Nat Neurosci 8,* 79-84.

27

12. Walsh, D. M., Klyubin, I., Fadeeva, J. V., Cullen, W. K., Anwyl, R., Wolfe, M. S., Rowan, M. J., and Selkoe, D. J. (2002) Naturally secreted oligomers of amyloid beta protein potently inhibit hippocampal long-term potentiation in vivo, *Nature 416*, 535-539.

13. Benilova, I., Karran, E., and De Strooper, B. (2012) The toxic Abeta oligomer and Alzheimer's disease: an emperor in need of clothes, *Nat Neurosci 15*, 349-357.

14. Lee, S. J., Nam, E., Lee, H. J., Savelieff, M. G., and Lim, M. H. (2017) Towards an understanding of amyloid-beta oligomers: characterization, toxicity mechanisms, and inhibitors, *Chem Soc Rev 46*, 310-323.

15. Leon, R., Garcia, A. G., and Marco-Contelles, J. (2013) Recent advances in the multitarget-directed ligands approach for the treatment of Alzheimer's disease, *Med Res Rev 33*, 139-189.

16. Di Martino, R. M. C., Bisi, A., Rampa, A., Gobbi, S., and Belluti, F. (2017) Recent progress on curcumin-based therapeutics: a patent review (2012-2016). Part II: curcumin derivatives in cancer and neurodegeneration, *Expert Opin Ther Pat 27*, 953-965.

17. Esatbeyoglu, T., Huebbe, P., Ernst, I. M., Chin, D., Wagner, A. E., and Rimbach, G. (2012) Curcumin--from molecule to biological function, *Angew Chem Int Ed Engl 51*, 5308-5332.

18. Prasad, S., Gupta, S. C., Tyagi, A. K., and Aggarwal, B. B. (2014) Curcumin, a component of golden spice: from bedside to bench and back, *Biotechnol Adv 32,* 1053-1064.

19. Masuda, Y., Fukuchi, M., Yatagawa, T., Tada, M., Takeda, K., Irie, K., Akagi, K., Monobe, Y., Imazawa, T., and Takegoshi, K. (2011) Solid-state NMR analysis of interaction sites of curcumin and 42-residue amyloid beta-protein fibrils, *Bioorg Med Chem 19*, 5967-5974.

20. Zhao, L. N., Chiu, S. W., Benoit, J., Chew, L. Y., and Mu, Y. (2012) The effect of curcumin on the stability of Abeta dimers, *J Phys Chem B 116*, 7428-7435.

21. Zhang, X., Tian, Y., Li, Z., Tian, X., Sun, H., Liu, H., Moore, A., and Ran, C. (2013) Design and synthesis of curcumin analogues for in vivo fluorescence imaging and inhibiting copper-induced cross-linking of amyloid beta species in Alzheimer's disease, *J Am Chem Soc 135*, 16397-16409.

22. Orlando, R. A., Gonzales, A. M., Royer, R. E., Deck, L. M., and Vander Jagt, D. L. (2012) A chemical analog of curcumin as an improved inhibitor of amyloid Abeta oligomerization, *PLoS One 7*, e31869.

23. Reinke, A. A., and Gestwicki, J. E. (2007) Structure-activity relationships of amyloid beta-aggregation inhibitors based on curcumin: influence of linker length and flexibility, *Chem Biol Drug Des 70,* 206-215.

24. Nelson, K. M., Dahlin, J. L., Bisson, J., Graham, J., Pauli, G. F., and Walters, M. A. (2017) The Essential Medicinal Chemistry of Curcumin, *J Med Chem 60*, 1620-1637.

25. Baell, J., and Walters, M. A. (2014) Chemistry: Chemical con artists foil drug discovery, *Nature 513,* 481-483.

26. Jasial, S., Hu, Y., and Bajorath, J. (2017) How Frequently Are Pan-Assay Interference Compounds Active? Large-Scale Analysis of Screening Data Reveals Diverse Activity Profiles, Low Global Hit Frequency, and Many Consistently Inactive Compounds, *J Med Chem 60*, 3879-3886.

27. Chojnacki, J. E., Liu, K., Yan, X., Toldo, S., Selden, T., Estrada, M., Rodriguez-Franco, M. I., Halquist, M. S., Ye, D., and Zhang, S. (2014) Discovery of 5-(4-hydroxyphenyl)-3-oxo-pentanoic acid [2-(5-methoxy-1H-indol-3-yl)-ethyl]-amide as a neuroprotectant for Alzheimer's disease by hybridization of curcumin and melatonin, *ACS Chem Neurosci 5*, 690-699.

28. Di Martino, R. M., De Simone, A., Andrisano, V., Bisignano, P., Bisi, A., Gobbi, S., Rampa, A., Fato, R., Bergamini, C., Perez, D. I., Martinez, A., Bottegoni, G., Cavalli, A., and Belluti, F. (2016) Versatility of the Curcumin Scaffold: Discovery of Potent and Balanced Dual BACE-1 and GSK-3beta Inhibitors, *J Med Chem 59*, 531-544.

29. Kuzuyama, T., Noel, J. P., and Richard, S. B. (2005) Structural basis for the promiscuous biosynthetic prenylation of aromatic natural products, *Nature 435*, 983-987.

30. Brezani, V., Smejkal, K., Hosek, J., and Tomasova, V. (2018) Anti-inflammatory Natural Prenylated Phenolic Compounds - Potential Lead Substances, *Curr Med Chem 25,* 1094-1159.

31. Marchiani, A., Rozzo, C., Fadda, A., Delogu, G., and Ruzza, P. (2014) Curcumin and curcumin-like molecules: from spice to drugs, *Curr Med Chem 21,* 204-222.

32. Pabon, H. J. J. A synthesis of curcumin and related compounds. *Recl Trav Chim Pay B 83,* 379-386.

33. Mercanti, G., Ragazzi, E., Toffano, G., Giusti, P., and Zusso, M. (2014) Phosphatidylserine and curcumin act synergistically to down-regulate release of interleukin-1beta from lipopolysaccharide-stimulated cortical primary microglial cells, *CNS Neurol Disord Drug Targets 13*, 792-800.

34. Bisceglia, F., Natalello, A., Serafini, M. M., Colombo, R., Verga, L., Lanni, C., and De Lorenzi, E. (2018) An integrated strategy to correlate aggregation state, structure and toxicity of Ass 1-42 oligomers, *Talanta 188,* 17-26.

35. Sabella, S., Quaglia, M., Lanni, C., Racchi, M., Govoni, S., Caccialanza, G., Calligaro, A., Bellotti, V., and De Lorenzi, E. (2004) Capillary electrophoresis studies on the aggregation process of beta-amyloid 1-42 and 1-40 peptides, *Electrophoresis 25*, 3186-3194.

36. Colombo, R., Carotti, A., Catto, M., Racchi, M., Lanni, C., Verga, L., Caccialanza, G., and De Lorenzi, E. (2009) CE can identify small molecules that selectively target soluble oligomers of amyloid beta protein and display antifibrillogenic activity, *Electrophoresis 30*, 1418-1429.

37. Butini, S., Brindisi, M., Brogi, S., Maramai, S., Guarino, E., Panico, A., Saxena, A., Chauhan, V., Colombo, R., Verga, L., De Lorenzi, E., Bartolini, M., Andrisano, V., Novellino, E., Campiani, G., and Gemma, S. (2013) Multifunctional cholinesterase and amyloid Beta fibrillization modulators. Synthesis and biological investigation, *ACS Med Chem Lett 4*, 1178-1182.

38. Brinet, D., Gaie-Levrel, F., Delatour, V., Kaffy, J., Ongeri, S., and Taverna, M. (2017) In vitro monitoring of amyloid beta-peptide oligomerization by Electrospray differential mobility analysis: An alternative tool to evaluate Alzheimer's disease drug candidates, *Talanta 35,* 84-91.

39. Bartolini, M., Bertucci, C., Bolognesi, M. L., Cavalli, A., Melchiorre, C., and Andrisano, V. (2007) Insight into the kinetic of amyloid beta (1-42) peptide self-aggregation: elucidation of inhibitors' mechanism of action, *Chembiochem 8*, 2152-2161.

40. Hudson, S. A., Ecroyd, H., Kee, T. W., and Carver, J. A. (2009) The thioflavin T fluorescence assay for amyloid fibril detection can be biased by the presence of exogenous compounds, *FEBS J 279,* 5960-5972.

41. Thapa, A., Jett, S. D., and Chi, E. Y. (2016) Curcumin Attenuates Amyloid-beta Aggregate Toxicity and Modulates Amyloid-beta Aggregation Pathway, *ACS Chem Neurosci 7*, 56-68.

42. Necula, M., Kayed, R., Milton, S., and Glabe, C. G. (2007) Small molecule inhibitors of aggregation indicate that amyloid beta oligomerization and fibrillization pathways are independent and distinct, *J Biol Chem 282*, 10311-10324.

43. Zusso, M., Mercanti, G., Belluti, F., Di Martino, R. M. C., Pagetta, A., Marinelli, C., Brun, P., Ragazzi, E., Lo, R., Stifani, S., Giusti, P., and Moro, S. (2017) Phenolic 1,3-diketones attenuate lipopolysaccharide-induced inflammatory response by an alternative magnesium-mediated mechanism, *Br J Pharmacol 174*, 1090-1103.

44. Baird, L., and Dinkova-Kostova, A. T. (2011) The cytoprotective role of the Keap1-Nrf2 pathway, *Arch Toxicol 85*, 241-272.

45. Ahmed, S. M., Luo, L., Namani, A., Wang, X. J., and Tang, X. (2017) Nrf2 signaling pathway: Pivotal roles in inflammation, *Biochim Biophys Acta 1863,* 585-597.

46. Pandima Devi, K., Rajavel, T., Daglia, M., Nabavi, S. F., Bishayee, A., and Nabavi, S. M. (2017) Targeting miRNAs by polyphenols: Novel therapeutic strategy for cancer, *Semin Cancer Biol 46,* 146-157.

47. Liu, Z., Tang, L., Zou, P., Zhang, Y., Wang, Z., Fang, Q., Jiang, L., Chen, G., Xu, Z., Zhang, H., and Liang, G. (2014) Synthesis and biological evaluation of allylated and prenylated mono-carbonyl analogs of curcumin as anti-inflammatory agents, *Eur J Med Chem 74*, 671-682.

48. Vistoli, G., Colzani, M., Mazzolari, A., Maddis, D. D., Grazioso, G., Pedretti, A., Carini, M., and Aldini, G. (2016) Computational approaches in the rational design of improved carbonyl quenchers: focus on histidine containing dipeptides, *Future Med Chem 8*, 1721-1737.

49. Rao, P. P., Mohamed, T., Teckwani, K., and Tin, G. (2015) Curcumin Binding to Beta Amyloid: A Computational Study, *Chem Biol Drug Des 86*, 813-820.

50. Korb, O., Stutzle, T., and Exner, T. E. (2009) Empirical scoring functions for advanced protein-ligand docking with PLANTS, *J Chem Inf Model 49,* 84-96.

51. Mashiach, E., Schneidman-Duhovny, D., Andrusier, N., Nussinov, R., and Wolfson, H. J. (2008) FireDock: a web server for fast interaction refinement in molecular docking, *Nucleic Acids Res 36*, W229-232.

52. Vistoli, G., Treumann, A., Zglinicki, T., and Miwa, S. (2016) Data from molecular dynamics simulations in support of the role of human CES1 in the hydrolysis of Amplex Red, *Data Brief 6*, 865-870.

53. Skaper, S. D., Argentini, C., and Barbierato, M. (2012) Culture of neonatal rodent microglia, astrocytes, and oligodendrocytes from cortex and spinal cord, *Methods Mol Biol 846*, 67-77.
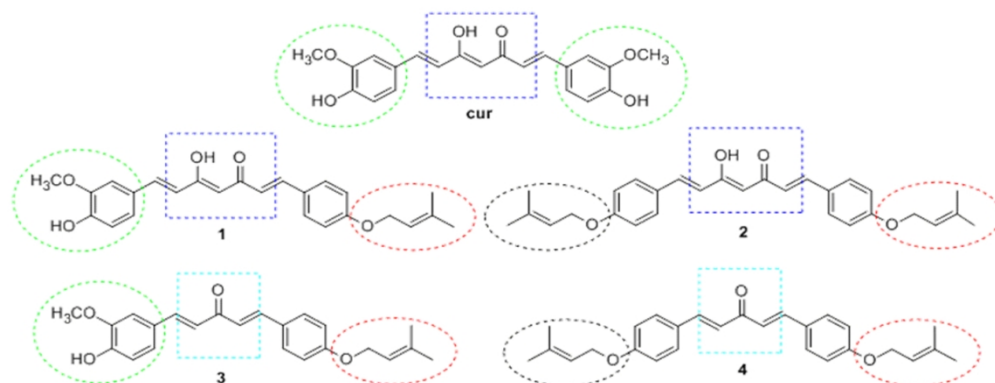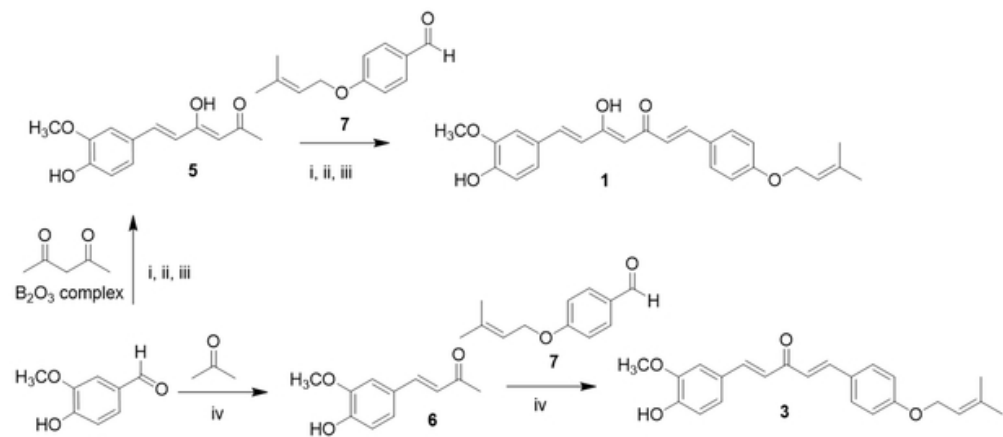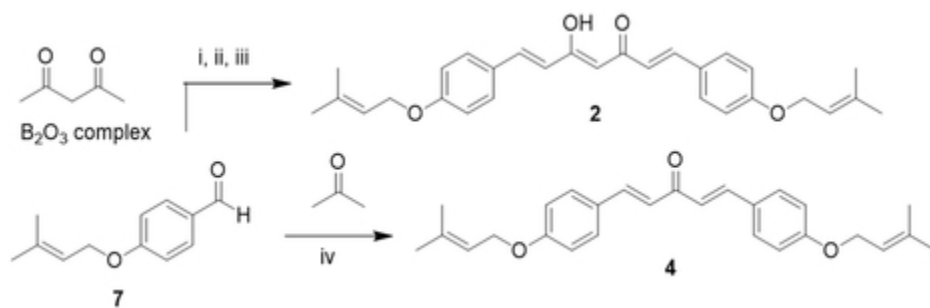
Figure 1. Design strategy toward the curcumin-based analogues **1-4**. Structures of curcumin (**cur**), the newly synthesized curcuminoids (**1**, **2**) and their monocarbonyl analogues (**3**, **4**).

119x50mm (300 x 300 DPI)

Scheme 1. Reagents and conditions: i) B(*n*-BuO)$_3$; ii) *n*-BuNH$_2$, 80 °C; iii) HCl, 80 °C; iv) KOH 50%. EtOH, rt.
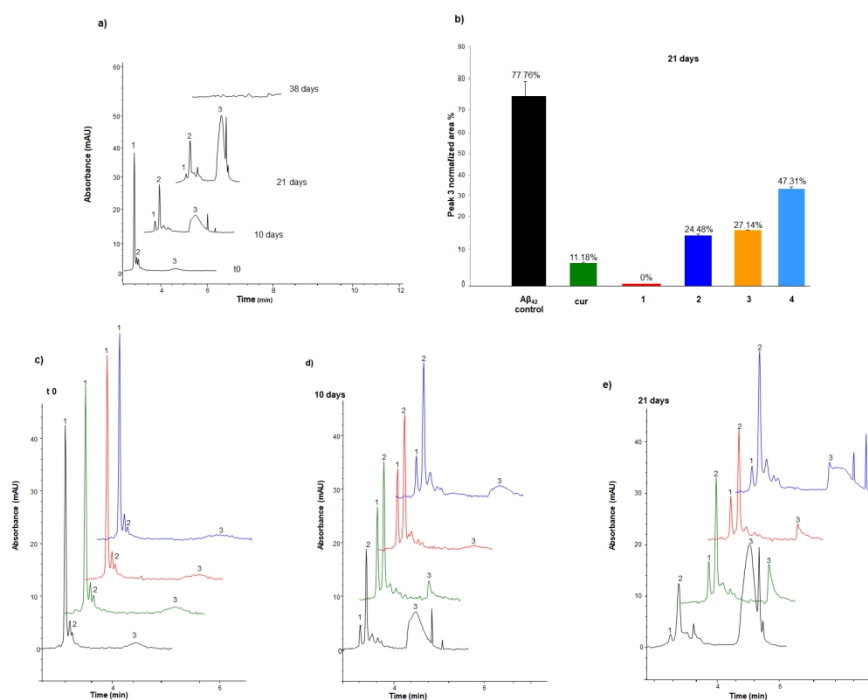
51x22mm (300 x 300 DPI)

Scheme 2. Reagents and conditions: i) B(n-BuO)$_3$; ii) n-BuNH$_2$, 80 °C; iii) HCl, 80 °C; iv) KOH 50%. EtOH, rt.

39x13mm (300 x 300 DPI)

Figure 2. Oligomerization of 100 µM Aβ$_{42}$ in the absence or in the presence of **cur** and of compounds **1–4**. a) Electrophoretic profiles of Aβ$_{42}$ control (solubilized in 3.26% EtOH in 20 mM phosphate buffer pH 7.4, see Experimental section) at selected elapsed times from t0 until precipitation: monitoring over time by CE. b) Anti-aggregation activity of 50 µM **cur** and compounds **1–4**: normalized area % of peak 3 at 21 days from sample redissolution as observed in control peptide and in the presence of compounds. Data are expressed as mean ± standard deviation, for n=3. c-e) Comparison between electrophoretic profiles of 100 µM Aβ$_{42}$ control (black trace) and in the presence of 10 µM **cur** (green traces), **1** (red traces) and **2** (blue traces) at different elapsed times from redissolution. Electropherograms are representative of n=3.
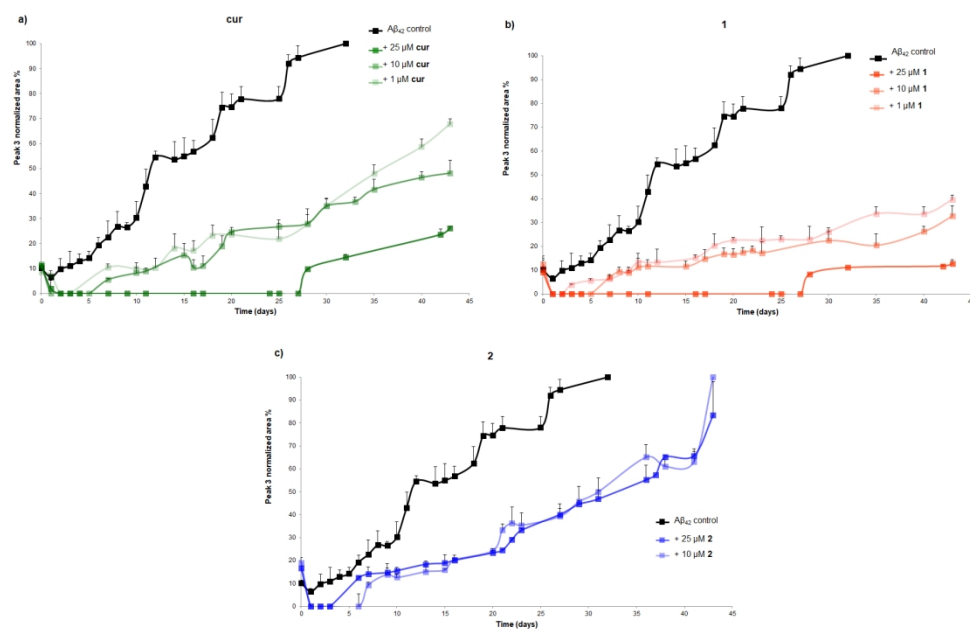
160x119mm (300 x 300 DPI)

Figure 3. Anti-oligomeric effect of compounds on toxic large oligomers (peak 3) over time. Normalized area percentage plot of peak 3 of 100 μM Aβ$_{42}$ control and in the presence of decreasing concentrations of: a) **cur**, b) **1**, c) **2**. Data are expressed as mean± standard deviation, for n=3.
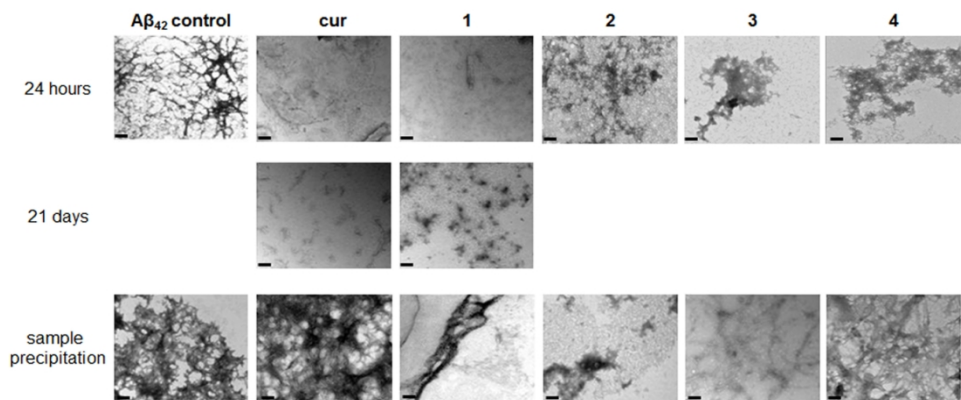
160x106mm (300 x 300 DPI)

Figure 4. TEM images of Aβ$_{42}$ control peptide (100 μM) and 100 μM Aβ$_{42}$ coincubated with 50 μM **cur** and **1-4** analyzed at different times from redissolution. Scale bar=100nm. 60000x. n=3

119x50mm (300 x 300 DPI)

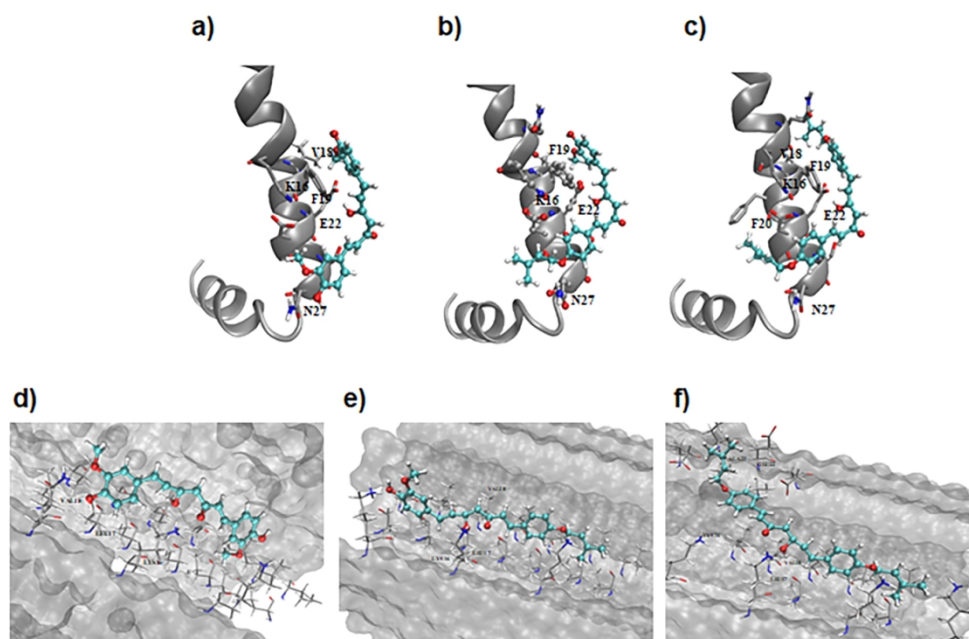Figure 5. Main interactions stabilizing the putative complexes with monomeric Aβ$_{42}$ for a) **cur**, b) **1** and c) **2**, and with the amyloid fibril structure for d) **cur**, e) **1** and f) **2**.
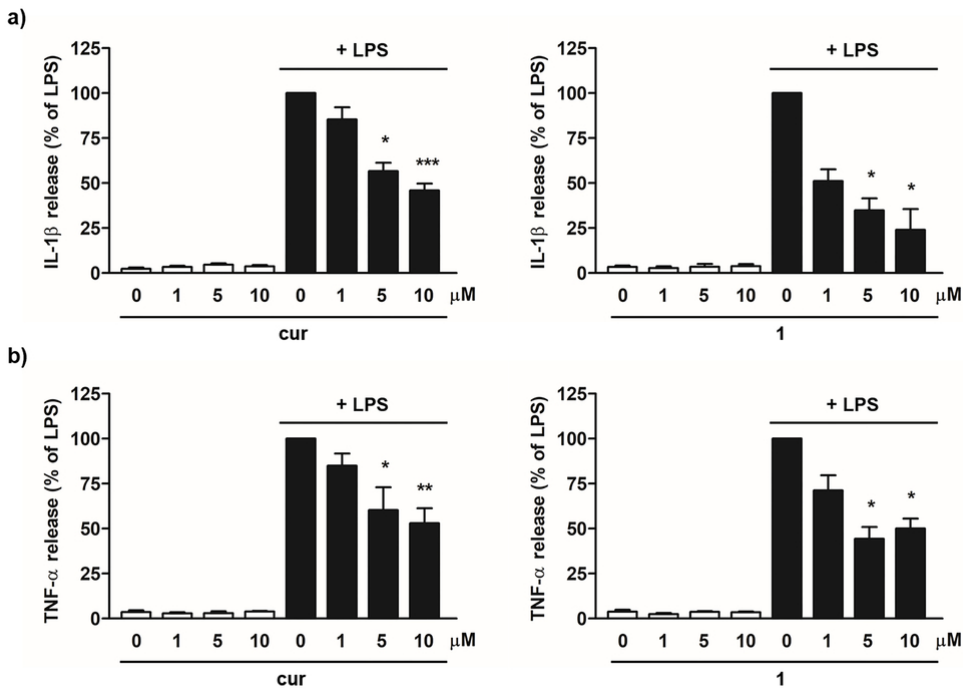
119x79mm (300 x 300 DPI)

Figure 6. Effects of **cur** and analogue **1** on cytokine release from LPS-stimulated cortical microglia cells. a) IL-1β and b) TNF-α release. Data are mean ± SEM (standard error of mean) (n=3). * p<0.05, ** p<0.01 and *** p<0.001 vs LPS-stimulated cultures, Kruskal-Wallis followed by post-hoc Dunn's test.
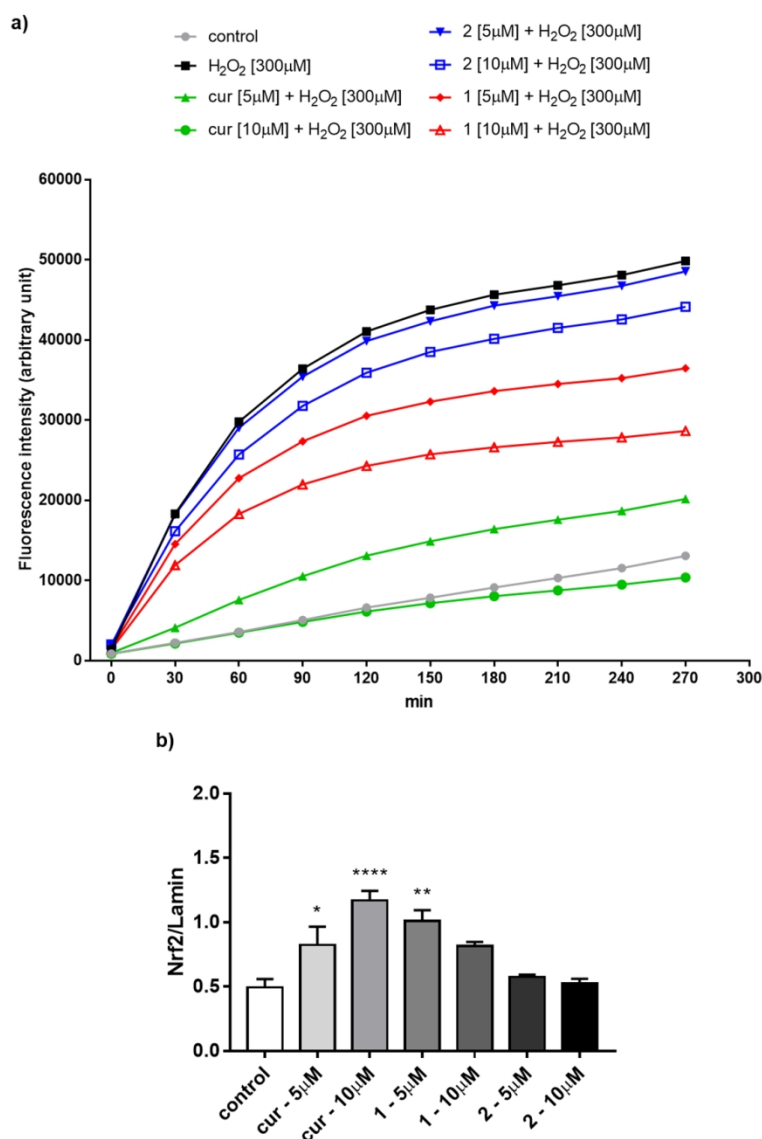
84x59mm (300 x 300 DPI)

Figure 7. Anti-oxidant activity of **cur** and analogues **1** and **2**. a) Reduction of H_2O_2-induced intracellular ROS production: fluorescence intensity for all compounds is significant at any time from 30 to 270 min with $p<0.001$ vs H_2O_2, with exception of compound **2** at the concentration of 5 µM. For compound **2** the significance is as follows: $p<0.05$ at 90 min; $p<0.01$ at 120 min and 270 min; $p<0.001$ at 150, 180, 210 and 240 min. Dunnett's multiple comparison test; b) Activation of Nrf2 pathway: SH-SY5H cells were treated for 3 hours with compounds. Results are shown as ratio Nrf2/lamin ± SEM; *$p < 0.05$, **$p < 0.01$, ****$p<0.0001$ versus control; Dunnett's multiple comparison test.

99x150mm (300 x 300 DPI)